

Spring 2010

# Experimental investigation of flow and heat transfer characteristics of R - 134A in microchannels

Abdullahel Bari  
*Louisiana Tech University*

Follow this and additional works at: <https://digitalcommons.latech.edu/dissertations>



Part of the [Mechanical Engineering Commons](#)

---

## Recommended Citation

Bari, Abdullahel, "" (2010). *Dissertation*. 716.  
<https://digitalcommons.latech.edu/dissertations/716>

This Dissertation is brought to you for free and open access by the Graduate School at Louisiana Tech Digital Commons. It has been accepted for inclusion in Doctoral Dissertations by an authorized administrator of Louisiana Tech Digital Commons. For more information, please contact [digitalcommons@latech.edu](mailto:digitalcommons@latech.edu).

## INFORMATION TO USERS

This manuscript has been reproduced from the microfilm master. UMI films the text directly from the original or copy submitted. Thus, some thesis and dissertation copies are in typewriter face, while others may be from any type of computer printer.

**The quality of this reproduction is dependent upon the quality of the copy submitted.** Broken or indistinct print, colored or poor quality illustrations and photographs, print bleedthrough, substandard margins, and improper alignment can adversely affect reproduction.

In the unlikely event that the author did not send UMI a complete manuscript and there are missing pages, these will be noted. Also, if unauthorized copyright material had to be removed, a note will indicate the deletion.

Oversize materials (e.g., maps, drawings, charts) are reproduced by sectioning the original, beginning at the upper left-hand corner and continuing from left to right in equal sections with small overlaps. Each original is also photographed in one exposure and is included in reduced form at the back of the book.

Photographs included in the original manuscript have been reproduced xerographically in this copy. Higher quality 6" x 9" black and white photographic prints are available for any photographs or illustrations appearing in this copy for an additional charge. Contact UMI directly to order.

**UMI<sup>®</sup>**

Bell & Howell Information and Learning  
300 North Zeeb Road, Ann Arbor, MI 48106-1346 USA  
800-521-0600



## **NOTE TO USERS**

**This reproduction is the best copy available.**

**UMI**



**EXPERIMENTAL INVESTIGATION OF FLOW  
AND HEAT TRANSFER CHARACTERISTICS  
OF R-134A IN MICROCHANNELS**

by

**Abdullahel Bari, MSME**

**A Dissertation Presented in Partial Fulfillment  
of the Requirements for the Degree  
Doctor of Engineering**

**COLLEGE OF ENGINEERING AND SCIENCE  
LOUISIANA TECH UNIVERSITY**

**May 2001**

UMI Number: 3004041

UMI<sup>®</sup>

---

UMI Microform 3004041

Copyright 2001 by Bell & Howell Information and Learning Company.

All rights reserved. This microform edition is protected against  
unauthorized copying under Title 17, United States Code.

---

Bell & Howell Information and Learning Company  
300 North Zeeb Road  
P.O. Box 1346  
Ann Arbor, MI 48106-1346

LOUISIANA TECH UNIVERSITY

THE GRADUATE SCHOOL

March 13, 2001

Date

We hereby recommend that the dissertation prepared under our supervision by

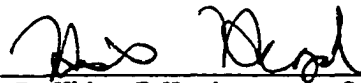
Abdullahel Bari

entitled EXPERIMENTAL INVESTIGATION OF FLOW AND HEAT TRANSFER

CHARACTERISTICS OF R-134A IN MICROCHANNELS

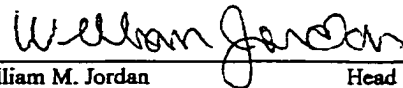
be accepted in partial fulfillment of the requirements for the Degree of     

Doctor of Engineering



Dr. Hisham E. Hegab

Supervisor of Thesis Research



Dr. William M. Jordan

Head of Department

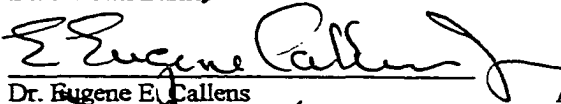
Mechanical Engineering

Department

Recommendation concurred in:



Dr. Mark Barker



Dr. Eugene E. Callens

Advisory Committee



Dr. Bill B. Elmore



Dr. Leslie K. Guice

Approved:

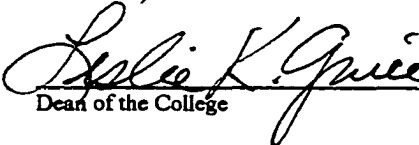


Director of Graduate Studies

Approved:



Dean of the Graduate School



Dean of the College

GS Form 13  
(1/00)



## ABSTRACT

The purpose of this study was to investigate the flow and heat transfer characteristics of liquid refrigerant R-134a in rectangular microchannels. The research concentrated mostly upon single-phase experiments with limited investigation of boiling phenomenon in microchannels. Tests were performed using rectangular microchannels with hydraulic diameters ranging from 112  $\mu\text{m}$  to 210  $\mu\text{m}$  and aspect ratios varying approximately from 1.0 to 1.5. The Reynolds number in the experiments ranged from 1,200 to 13,000 although most data were collected in the transition and turbulent flow regimes.

The experimental data for friction factor measurement had a similar trend as predicted by macroscale theory but with consistently lower values of friction factor. The uncertainty associated with friction factor measurement varied from 3% to 23.3% for all of the four channel configurations studied, whereas the Reynolds number uncertainty was within 10% for all measurements. The experimental data provided an excellent correlation to predict friction factor for  $Re > 4000$ . The heat transfer rate and Nusselt number were found to be much lower, ranging from 5% to 84% lower than theoretical predictions while the uncertainty associated with Nusselt number varied from 20% to 67%, approximately. Two different modes of heat transfer were observed, the larger channels providing a much higher rate of heat transfer compared

with the two smaller configurations. A maximum heat flux of  $16 \text{ W/cm}^2$  was achieved in single-phase experiments associated with a pressure drop of about 653 kPa.

## APPROVAL FOR SCHOLARLY DISSEMINATION

The author grants to the Prescott Memorial Library of Louisiana Tech University the right to reproduce, by appropriate methods, upon request, any or all portions of this Dissertation. It is understood that "proper request" consists of the agreement, on the part of the requesting party, that said reproduction is for his personal use and that subsequent reproduction will not occur without written approval of the author of this Dissertation. Further, any portions of the Dissertation used in books, papers, and other works must be appropriately referenced to this Dissertation.

Finally, the author of this Dissertation reserves the right to publish freely, in the literature, at any time, any or all portions of this Dissertation.

Author Abdullahel Bar<sup>1</sup>

Date 5/16/01

## TABLE OF CONTENTS

	Page
ABSTRACT .....	iii
LIST OF TABLES .....	vii
LIST OF FIGURES .....	viii
ACKNOWLEDGMENTS .....	x
CHAPTER 1: INTRODUCTION.....	1
CHAPTER 2: LITERATURE REVIEW .....	4
Single-Phase Flow in Microchannels .....	4
Flow Boiling in Microchannels .....	14
CHAPTER 3: THEORY.....	22
Single-Phase Flow .....	22
Laminar Flow .....	22
Turbulent Flow .....	25
Boiling and Two-Phase Flow .....	28
Pool Boiling.....	29
Flow Boiling.....	34
CHAPTER 4: EXPERIMENTAL SET-UP AND PROCEDURE .....	38
Experimental Apparatus .....	38
Test Section .....	38

Test Fixture.....	48
Flow Loop .....	51
Experimental Procedure .....	55
Data Reduction Technique .....	61
Error Analysis.....	65
Precision Error.....	66
Bias Error.....	67
CHAPTER 5: ANALYSIS OF RESULTS.....	70
Single-Phase Flow.....	70
Friction Factor .....	70
Nusselt Number .....	72
Two-Phase Flow .....	76
CHAPTER 6: CONCLUSIONS AND RECOMMENDATIONS.....	89
Summary of Present Study .....	89
Recommendations for Future Research.....	93
APPENDIX : EXPERIMENTAL DATA .....	94
BIBLIOGRAPHY .....	103
VITA.....	108

## LIST OF TABLES

Table 4.1: Measured Microchannel Dimensions .....	40
Table 4.2: Thermal and Mechanical Properties of Experimental Apparatus Materials .....	50
Table 4.3: Bias Error for Measured Experimental Variables .....	69

## LIST OF FIGURES

Figure 3.1: Boiling curve of water (Incropera and DeWitt, 1990).....	29
Figure 3.2: Flow regimes in a two-phase flow (Tong et al. 1997) .....	33
Figure 3.3: Flow Regime Map for horizontal flow (Tong et al. 1997) .....	37
Figure 4.1: Test Section; (a) Dimensions, (b) Cross-section, (c) Component description, and (d) Thermocouple locations and numbering, Approximately 0.01” beneath channels.....	42
Figure 4.2: Mathematical model to determine channel spacing .....	44
Figure 4.3: Test fixture assembly.....	49
Figure 4.4: Schematic of experimental flow loop.....	52
Figure 4.5: General layout of floe loop components .....	54
Figure 4.6: General layout of entire flow loop apparatus .....	54
Figure 4.7: Test fixture components .....	56
Figure 4.8: Complete view of test fixture .....	56
Figure 4.9: Detail of test fixture components without test section .....	57
Figure 4.10: Detail of test fixture without test section installed .....	57
Figure 5.1: Friction factor for channel configuration B.....	78
Figure 5.2: Friction factor for channel configuration C1 .....	79
Figure 5.3: Friction factor for channel configuration C2.....	80
Figure 5.4: Friction factor for channel configuration D.....	81
Figure 5.5: Friction factor comparison with Choi (1991) and Yu (1994)’s data....	82

Figure 5.6: Curvefit of the experimental data .....	83
Figure 5.7: Nusselt number for channel configuration B.....	84
Figure 5.8: Nusselt number for channel configuration C1.....	85
Figure 5.9: Nusselt number for channel configuration C2.....	86
Figure 5.10: Nusselt number for channel configuration D .....	87
Figure 5.11: Nusselt number comparison with Peng et al. (1994)'s data .....	88



## **ACKNOWLEDGMENTS**

I would like to thank my mother, Mrs. Amina Begum, for her untiring support throughout the course of this study. I would also like to thank Dr. Hisham E. Hegab for being my supervisor. This work could not have been accomplished without his guidance and support at every phase of the research. I would also like to thank my other committee members, Dr. J. Mark Barker, Dr. Eugene E. Callens, and Dr. Bill B. Elmore as well for their invaluable suggestions during my research. I also appreciate the help and support that I received from Mr. Murray Rasbury and Mr. Jimmy Cook in the machine shop in the past five years and also from Lillian during writing this dissertation.

Last, but not the least, I would like to thank my wife Imrana and daughter Tahsin for being patient and understanding as I spent hours for research and writing this dissertation.

# CHAPTER 1

## INTRODUCTION

Developments in microfabrication technology have made possible extreme miniaturization of electronic devices and electromechanical equipment. On the other hand, advancements in semi-conductor technology with the introduction of high-speed, high-density ULSI and VLSI circuits has led to an ever-increasing requirement for effective and compact heat removal to ensure optimum operating temperatures, leading to enhancement in chip reliability (Peterson *et al.*, 1993). Forced convection air cooling is currently employed for electronic chips and is limited to the order of 1 W/cm<sup>2</sup>, whereas chip power dissipation levels of 100 W/cm<sup>2</sup> are anticipated in the near future (Mallik *et al.*, 1992). To attain this goal, liquid cooling by dielectrics may be required. With normal pool boiling, inert dielectric liquids are capable of handling heat fluxes on the order of 10 W/cm<sup>2</sup> and with surface enhancements heat fluxes above 100 W/cm<sup>2</sup> can be achieved (Orozco and Hanson, 1992). Although several investigators, including Tuckerman and Pease (1981) and Bowers and Mudawar (1994) reported that greater heat removal rates (10<sup>3</sup> W/cm<sup>2</sup> – 10<sup>4</sup> W/cm<sup>2</sup>) can be achieved using water as a coolant, large pressure drops at high fluxes (about 100 kPa at 1.81x10<sup>2</sup> W/cm<sup>2</sup>) is the main limitation. Though numerous correlations have been developed and many investigations have been made regarding flow and heat transfer

characteristics of fluids flowing through macrochannels, very little is known about the validity of those correlations for microchannels. It is important to understand phenomena on the microscale so that they may be applied to new technologies such as micro heat exchangers, thin film deposition techniques etc. These applications suggest that there is a need for theoretical and experimental investigations of flow and heat transfer characteristics at the micro level. Microchannels are desirable for heat-dissipating devices because of their high surface area to volume ratio.

Although microfabrication techniques primarily evolved from the development of electronic circuits, application of these technologies has expanded into the fields of bioengineering such as separation of cells and blood flow through veins, aerospace, mini heaters and mini heat exchangers, material processing, thin-film deposition technologies, etc. It is anticipated that new applications will be identified in the near future.

A review of the pertinent literature indicates that most research efforts on fluid flow and heat transfer phenomena at the micro level deal mostly with single-phase flow, but very few investigations have been reported to date on two-phase and phase change/boiling heat transfer in microgeometries. Experimental results (Tuckerman and Pease, 1981; Bowers and Mudawar, 1994) indicate that a better heat-removal rate can be achieved in microchannels for single-phase flow compared with macrochannels. However, in practical applications, it is observed in macrochannels that a much higher rate of heat removal can be attained during phase change, due to the high latent heat of vaporization as opposed to single-phase heat transfer. During vaporization, the fluid temperature virtually remains constant; this uniformity of temperature reduces the

induced thermal stresses of the heating surface. Thus, it is of great interest to investigate whether the same trend is followed in microchannel heat transfer.

The objective of this research is an experimental investigation of flow and heat transfer characteristics of liquid refrigerant R-134a flowing through microchannels. This particular fluid was chosen as it is widely used in commercial applications because of its non-CFC configuration. This research concentrates on single-phase experiments with limited investigation of boiling phenomenon in microchannels. Though numerous investigations have been reported about single-phase experiments, different researchers have reported contradicting results. Also the present author is not aware of any research work using R-134a in microgeometries. In this report the friction factor, heat transfer coefficient, Nusselt number, and other related parameters have been determined for a range of flow conditions in microchannels with hydraulic diameters ranging from 112  $\mu\text{m}$  to 210  $\mu\text{m}$  and aspect ratios varying from 1.0 to 1.5. The effects of laminarity and turbulence on those parameters are also investigated.

These results are compared with existing empirical correlations available for macroscale flow. Further, an effort has been made to derive new empirical formulas based on the experimental data. It is expected that the research findings of this investigation will help to develop a better understanding of heat transfer phenomenon in microchannels.

## CHAPTER 2

### LITERATURE REVIEW

#### Single-Phase Flow in Microchannels

As the field of microfabrication technology continues to grow, it is becoming increasingly important to understand associated thermal and transport phenomena in microgeometries. One of the earliest microflow studies reported was conducted by Knudsen (1909). However, experiments were performed using capillary tubes and measurements were limited to global quantities due to non-availability of instruments with high precision and spatial resolution. No significant research was done in this area until Tuckerman and Pease (1981), in their pioneering research work, proposed that a much higher rate of heat transfer can be achieved for fluid flow in microchannels, thus enhancing the feasibility of ultrahigh-speed VLSI circuits. They determined the performance of a heat exchanger by measuring its thermal resistance  $\theta$ , where  $\theta = \Delta T/Q$ ,  $\Delta T$  is the temperature rise of the circuit above the input coolant temperature, and  $Q$  is the dissipated power. The total resistance was considered as a sum of three separate resistances, due to conduction, convection and heating of the coolant. Of the three components, the convective resistance was identified as the most dominant. Using the heat transfer coefficient  $h$ , from the definition of Nusselt number  $Nu$ ,  $h = k Nu/D$ , the only way to increase  $h$  for a particular fluid and a given flow

condition is to reduce  $D$ , the "characteristic width" of the channel since it increases the surface area to volume ratio. This observation is one justification for the investigation of microscopic channels. The local Nusselt number was calculated from the relation

$$\text{Nu}_x \sim (x/ D\text{RePr})^{-1/3}, \quad \text{for } x/(D\text{RePr}) \ll 0.02 \quad (2.1)$$

assuming a fully developed flow, where  $x$  is the distance from the entrance of the channel. The experiments were performed for 50  $\mu\text{m}$  wide and 300  $\mu\text{m}$  deep channels in silicon wafers with water as the coolant. For a temperature rise of 71°C, a heat transfer rate of  $7.9 \times 10^2 \text{ W/cm}^2$  was achieved.

Peng *et al.* (1994a, b) studied both frictional flow and heat transfer characteristics of water flowing through rectangular microchannels. The channels varied from 0.133 to 0.367 mm in hydraulic diameters and 0.333 to 1 in aspect ratios. They observed a strong dependence of critical Reynolds number for transition from laminar flow, decreasing with corresponding decreases in hydraulic diameter. Depending on channel size, laminar flow transition occurred at Reynolds number ranging from 200 to 700 and a fully developed turbulent flow was initiated at Reynolds number between 1000 and 1500. Based on their experimental data, the following expressions were proposed for friction factor

$$f = C_{f,l}/\text{Re}^{1.98} \quad \text{for laminar flow} \quad (2.2a)$$

$$f = C_{f,t}/\text{Re}^{1.72} \quad \text{for turbulent flow} \quad (2.2b)$$

where  $C_{f,l}$  and  $C_{f,t}$  are coefficients based on experimental results. The product of the friction factor and Reynolds number was found to be constant for a particular channel geometry and was usually less than 64, the theoretical value for laminar flow in macrosized tubes. Peng et al. (1994a, b) also proposed a new correlation for forced convective heat transfer given by

$$\text{Nu} = C_{H,l} \text{Re}^{0.62} \text{Pr}^{1/3} \quad \text{for laminar flow} \quad (2.3a)$$

where  $C_{H,l}$  is an empirical coefficient based on geometric parameters of the channel. Peng et al. (1994a, b) also proposed the following correlation

$$\text{Nu} = C_{H,t} \text{Re}^{0.8} \text{Pr}^{1/3} \quad \text{for turbulent flow} \quad (2.3b)$$

where  $C_{H,t}$  was experimentally determined. This latter correlation may be compared with the Colburn equation, a typical macrochannel correlation,

$$\text{Nu} = 0.023 \text{Re}^{0.8} \text{Pr}^{1/3} \quad (2.4)$$

which incorporates a different empirical coefficient and thus predicts a much higher Nusselt number than the experimental data of Peng. Peng *et al.* (1994a, b) also reported that the heat transfer coefficient for laminar flow through microchannels might be higher than that for turbulent flow in conventional macrochannels at equivalent Reynolds number.

In a later study, Peng and Peterson (1996) conducted a similar investigation in microchannels with hydraulic diameters ranging from 0.133 to 0.367 mm, and aspect ratios ranging from 0.5 to 3.0, to determine the effect of geometric configuration on

flow and heat transfer characteristics. In addition to the aspect ratio (height  $H$  /width  $W$ ), they proposed a new dimensionless variable  $Z$ , a critical parameter in the determination of the empirical coefficients in equation 2.3a and 2.3b. Also the turbulent heat transfer was found to be a function of  $Z$ , such that  $Z = 0.5$  was the optimum configuration for turbulent heat transfer.  $Z$  was defined as

$$Z = \frac{\min(H,W)}{\max(H,W)} \quad (2.5)$$

Based on the experimental results they recommended the following expressions for the empirical coefficients in equation 2.3a and 2.3b.

$$C_{H,i} = 0.1165 \left( \frac{D_h}{W_c} \right)^{0.81} \left( \frac{H}{W} \right)^{-0.79} \quad (2.6)$$

$$C_{H,t} = 0.072 \left( \frac{D_h}{W_c} \right)^{1.15} \left[ 1 - 2.421(Z - 0.5)^2 \right] \quad (2.7)$$

where,  $D_h$  is the hydraulic diameter and  $W_c$  is the center-to-center distance of the microchannels in a channel blank.

Peng *et al.* (1995) also conducted an experimental investigation to determine the heat transfer characteristics and cooling performance of rectangular microchannels with methanol as the working fluid. Channels with different aspect ratios and a variety of center-to-center spacing were evaluated, and tests were conducted for both single-phase and flow boiling conditions. Liquid flow velocity, temperature and degree of subcooling were found to be important parameters for heat transfer and cooling performance.



Pfahler *et al.* (1990) conducted experiments in microchannels to determine the frictional flow characteristics of both liquids and gases for fully developed laminar flow. They used rectangular channels 100  $\mu\text{m}$  wide with depth varying from 0.5 to 4.65  $\mu\text{m}$ . The liquid flow was considered incompressible, but compressible flow occurred with the gas due to very high pressure gradients. However, being unable to find any pertinent theory on the calculation of friction factor for compressible flow, they used incompressible flow predictions. Based on experimental results, the friction law was prescribed as  $f^*Re=C_f$ , with  $C_f$  being independent of Reynolds number and consistently lower than the theoretical prediction. Pfahler *et al.* (1990) also reported that, for one particular case in a 3  $\mu\text{m}$  deep channel using silicone oil as the working fluid, the friction constant  $C_f$  increased linearly with Reynolds number. The authors could not explain this fact, but they suspected non-Newtonian behavior of the fluid and effects of channel size.

In a later study, Pfahler *et al.* (1991) performed similar experiments with different fluids in both rectangular and trapezoidal microchannels with depths ranging from 0.5  $\mu\text{m}$  to 50  $\mu\text{m}$ . The results indicated that the relationship between  $C_f$  and  $Re$  is affected by fluid species. Due to high pressure gradients (800 to 470,000 kPa/m) gas flow had to be considered compressible, which causes an accelerated flow due to reduction in density. This varying density or local gas temperature could not be measured directly with available instrumentation technology at that time. The flow was assumed to be fully developed. Though the normalized friction constant  $C^* = C_{f,\text{expt.}}/C_{f,\text{th.}}$  was found to decrease with decreasing channel depth for liquid flow, the exact opposite behavior was observed for gas flow, which the authors could not

explain satisfactorily. They proposed that higher temperatures in the smaller channels might have increased the viscosity of the gases, thus causing higher frictional resistance, which they indicated requires more analysis.

Papautsky *et al.* (1999) experimentally investigated the effects of rectangular microchannel aspect ratio on laminar friction factor. The channel widths varied from 150  $\mu\text{m}$  to 600  $\mu\text{m}$  and heights ranged from 22.71  $\mu\text{m}$  to 26.35  $\mu\text{m}$ . With water as the testing fluid, experiments were performed with Reynolds numbers ranging from 10 to 1000. For smaller channels with Reynolds numbers below 10, the friction factor was found to be 20% higher than macroscale predictions from the classical Navier-Stokes theory. A similar trend was observed when aspect ratios were 0.1 or less. However, the larger microchannels with characteristic dimensions on the order of 100  $\mu\text{m}$  and Reynolds numbers up to 1000 had friction factor values very close to the theoretical predictions. The authors could not decide whether it was the larger size of the channels or higher Reynolds number that minimized the microscale effects.

Flockhart and Dhariwal (1998) conducted both numerical and experimental investigations to determine the flow characteristics of trapezoidal channels with water as the test fluid. The channels were etched in silicon with hydraulic diameters ranging from 50 to 120  $\mu\text{m}$ . Their results indicated that for the channels considered, numerical analysis could adequately predict the flow characteristics of trapezoidal channels. Pressure drop across the channel and Poiseuille number are the parameters compared.

Harley *et al.* (1995) conducted theoretical and experimental investigations of compressible gas flow in microchannels. The channels were 100  $\mu\text{m}$  wide, 10 mm long, and 0.5 to 20  $\mu\text{m}$  deep and both rectangular and trapezoidal in cross-section. The

velocity profile was obtained using a “locally fully developed” approximation since this knowledge is required to calculate the friction factor from pressure measurements. Due to unavailability of appropriate sensors, temperatures and pressures were measured outside the test section. Because of the large aspect ratio ( $H/W$ ) of the channels investigated, analytical and numerical solutions were derived approximating flow between two parallel plates. The friction factor was found to be within 3% of the predicted value for isothermal, fully developed incompressible flow. But for low  $Re$ , Knudsen number ranged from 0.004 to 0.373 implying that the rarefaction effect could not be neglected. For choking conditions at the outlet, adiabatic flow was assumed near the choking point. In these cases too, results were within 8% of the predicted value.

Babin *et al.* (1990) conducted analytical and experimental investigations to identify the performance limitations and operating characteristics of trapezoidal micro heat pipes. They observed that channel angle and gravitational effects are important in determining the heat transport limits of trapezoidal channels.

Mallik *et al.* (1992) developed a transient three-dimensional numerical model to predict the effect of an array of 100  $\mu\text{m}$  diameter heat pipes incorporated into semiconductor chips. The numerical model can predict the temperature distribution, localized heat flux, and temperature gradients occurring within the chip. The results indicated significant reductions in chip temperature, thermal gradients, and localized heat fluxes.

Peterson *et al.* (1991, 1993) reported experimental results regarding thermal behavior of micro heat pipe arrays. For both rectangular and triangular heat pipes with

methanol as the working fluid, experimental results indicated that incorporating an array of micro heat pipes as an integral part of semiconductor devices significantly increases the heat transfer rates, decreases the maximum temperature and also the temperature gradients. Experimental results indicated that for the same number and cross-sectional array density, triangular heat pipes are significantly better than rectangular heat pipes in performance.

Kishimoto and Ohsaki (1986) described a method of indirect liquid cooling of VLSI chips. This method involves mounting VLSI chips on a multilayered alumina substrate, which incorporates very fine coolant channels with a cross-sectional area of less than 1 mm square. The cooling capability was tenfold greater than that obtained by conventional indirect water cooling.

Ma and Gerner (1993) developed a correlation for the average Nusselt number for forced convection heat transfer from microstructures. They suggested that thermal boundary layer theory is invalid for microstructures. Because the average thickness of the thermal boundary layer is of the same order as the length of the heated element, axial conduction (neglected in conventional boundary layer theory) needs to be considered.

Arkilic *et al.* (1994) investigated the effect of slip velocity on the mass flow prediction of the Navier-Stokes equation. It was observed that a slip flow boundary condition could accurately model the mass flow-pressure relationship for helium gas flow through microchannels.

Whereas most researchers concentrated on microchannels, Choi *et al.* (1991) were the first to investigate friction and heat transfer characteristics for fluid flow in

microtubes. Measurements were made for both laminar and turbulent flow with microtube diameters ranging from 3 to 81  $\mu\text{m}$  and with nitrogen gas as the working fluid. For laminar flow, friction factor was found to be less than that in conventional tubes at dynamically similar conditions, as opposed to the findings of some other researchers. The friction factor was also found to be independent of tube roughness for laminar flow. Based on experimental data, several correlations were proposed. Friction factor correlations are given by the following expressions:

$$f = \frac{64}{\text{Re}} \left[ 1 + 30 \left( \frac{\nu}{DC_a} \right) \right]^{-1} \quad \text{for laminar flow (Re < 2300)} \quad (2.8a)$$

and,

$$f = 0.14 \text{Re}^{-0.182} \quad \text{for turbulent flow (4000 < Re < 18,000)} \quad (2.8b)$$

where,  $\nu$  is the kinematic viscosity,  $D$  is the inside diameter of the microtube, and  $C_a$  is the acoustic velocity. The convective heat transfer data were correlated by the following relationships:

$$\text{Nu} = 0.000972 \text{Re}^{1.17} \text{Pr}^{1/3} \quad (\text{Re} < 2000) \quad (2.9a)$$

$$\text{Nu} = 3.82 \times 10^{-6} \text{Re}^{1.96} \text{Pr}^{1/3} \quad (2500 < \text{Re} < 20,000) \quad (2.9b)$$

Yu *et al.* (1994) conducted investigations similar to Choi *et al.* (1991), using both nitrogen gas and water with microtube diameters of 19, 52, and 102  $\mu\text{m}$ . Their results followed the same trend as Choi *et al.* (1991). The friction factor was found to be less than predicted by macroscale theory for both laminar and turbulent flow. Based on experimental results, they proposed the following correlations:

$$f = 50.13/Re \quad \text{for } Re < 2000 \quad (2.10a)$$

$$f = 0.302/ Re^{0.25} \quad \text{for } 6000 < Re < 20,000 \quad (2.10b)$$

The heat transfer was also enhanced in the turbulent regime, and the Nusselt number was much higher than predicted by conventional relations for a large tube, suggesting that the Reynolds analogy does not hold for microchannel flow. For micro turbulent flow, the following heat transfer correlation was recommended.

$$Nu = 0.007 Re^{1.2} Pr^{0.2} \quad \text{for } 6000 < Re < 20,000 \quad (2.11)$$

This heat transfer result contrasts with those reported by Peng *et al.* (1994a, b).

Webb and Zhang (1998) conducted single-phase flow and heat transfer experiments in channels with hydraulic diameter of 1.31 mm, using R-134a as the working fluid. The results agreed with empirical heat transfer and friction correlations. However, in absence of any established minimum size for microscale effects to take place, it is possible that the channels were too big to produce any deviation from standard correlations.

Adams *et al.* (1998) investigated turbulent, single-phase forced convection of water in circular microchannels. Two sets of microchannels were used with diameters of 0.76 and 1.09 mm. Their experimental data indicated a higher Nusselt number than those predicted by traditional large channel correlations. Based on their findings, they proposed a modification of the Gnielinski correlation of the following form to accommodate the small diameters encountered in microchannels.

$$Nu = Nu_{Gn}(1+F) \text{ and } F = C*Re[1 - (D/D_o)^2] \quad (2.12)$$

where  $C = 7.6E-05$  and  $D_0 = 1.164$  mm obtained from the least square fit of experimental data.  $D_0$  represents the diameter for which no enhancement of Nusselt number is predicted over that predicted by Gnielinski correlation.

Pong *et al.* (1994) measured the pressure distribution in microchannels for both nitrogen and helium. The pressure distribution as a function of distance from the channel entrance was found to be non-linear. The non-linearity increased with the inlet pressure level and was always accompanied by a large pressure drop across the channel. The non-linearity was possibly caused by a Knudsen number effect and also by compressibility due to high loss in pressure.

### **Flow Boiling in Microchannels**

Though most of the work done in microchannels has involved single-phase flow, boiling and two-phase flows have gained notable consideration in recent years due to the high flux associated with vaporization. Schonberg *et al.* (1995) numerically evaluated the heat flux of a steady evaporating meniscus, using a finite element procedure, kinetic theory, and the augmented Young-Laplace equation of capillarity. Heat fluxes in the range  $1.3$  to  $1.6 \times 10^2$  W/cm<sup>2</sup> were obtained based on channel width and apparent contact angle which was found to have a large effect on the heat transfer rate. Although the authors suggested that high heat flux might be obtained by a stable evaporating meniscus, pressure drop associated with the vapor removal would be substantial and needs special attention.

Peng and Wang (1994) introduced phase change into consideration and reported distinctly dissimilar characteristics to those of liquid forced convection and flow boiling in conventional macrochannels. Tests were performed for rectangular channels with widths ranging from 200-800  $\mu\text{m}$ , at a fixed depth of 700  $\mu\text{m}$ . Heat transfer in laminar and transition flow was found to be affected by inlet liquid temperature, velocity, and microchannel size in addition to the Reynolds number; however, these parameters had little significance in fully-developed turbulent flow. Although the authors reported that reduction in channel size would defer the onset of transition, they suggested more experimentation for verification of their results. The authors could not explain the observed phenomenon in which the heat transfer performance identically exhibited the characteristics of mixed convection. For mixed convective heat transfer to take place, theory suggests  $Gr/Re^2 \sim 1$  (Incropera and DeWitt, 1996); however, for their experimental condition where  $Gr/Re^2 < 0.005$ , forced convection should have been dominant. This finding suggests that more theoretical analyses as well as experimental investigations of liquid forced flow convection in microchannels be considered.

Throughout the experiments of Peng and Wang (1994) no vapor bubbles were seen in the microchannels, even for fully developed nucleate boiling. They suggested that the scale of the microchannels was smaller than the space required for bubble growth. But later the authors suggested (Peng, 1995) that there might actually be bubbles in the microchannels but that they were too small to be seen. The authors termed this phenomenon “phantom /fictitious boiling.”



Peng *et al.* (1998a) in a recent study investigated the boiling characteristics for liquids in microchannels by analyzing the thermodynamics of liquid phase transition. They suggested if the microchannel size is smaller than the “evaporating space,” then ‘fictitious boiling’ can be induced. Otherwise, normal nucleate boiling occurs. The term ‘fictitious boiling’ implies that although the liquid reached conventional nucleate boiling conditions, but internal evaporation and bubble growth may have not occurred, or there could be countless microbubbles within the liquid that cannot be visualized by ordinary means. However, the liquid still absorbs much more heat than possible by sensible heating. Using thermodynamic phase stability theory, a bubble formation nucleation criterion was obtained analytically. This criterion is represented by the following dimensionless parameter

$$N_{mb} = \frac{h_{lv}a_v}{c\pi(v''-v')q''D_h} \quad (2.13)$$

and the condition for liquid nucleation in microchannel was  $N_{mb} \leq 1$ . Here  $h_{lv}$  is enthalpy of vaporization,  $a_v$  is the thermal diffusivity of vapor,  $v''$  and  $v'$  are specific volumes of vapor and liquid respectively at saturation,  $q''$  is heat flux and  $c$  is an empirical constant determined from experiment. However, they suggested that the theoretical conclusions could be substantiated only by extensive experimental research.

In another study, Peng *et al.* (1995) investigated flow boiling of methanol in rectangular microchannels. It was observed that with a sufficiently high superheat, flow boiling was initiated at once and immediately developed into fully developed nucleate boiling. It was also reported that no partial nucleate regime existed even with

a high liquid subcooling. This rapid change to fully developed nucleate flow boiling greatly enhanced the heat removal rate, a behavior significantly different from that observed in subcooled flow boiling in larger channels. Their experiments indicated that liquid velocity and subcooling had little effect on the boiling initiation.

In a later study Peng *et al.* (1998b) performed an experimental investigation of flow and boiling heat transfer characteristics of water and methanol flowing through V-shape microchannels. The channels had hydraulic diameters ranging from 0.2 to 0.6 mm and V-shaped groove angles from 30 to 60 degrees. Results indicated that there exist both an optimum hydraulic diameter and an optimum groove angle to initiate the boiling process. They also noted that fully nucleate boiling was influenced by liquid flow velocity, in contradiction to the previous results of Peng *et al.* (1995).

Lin *et al.* (1993) experimentally investigated the formation of vapor bubbles in confined and unconfined microchannels of trapezoidal cross-sections between 30 and 60  $\mu\text{m}$  in width and 7.5  $\mu\text{m}$  in depth. For all three liquids considered, bubble formation temperature was found experimentally to be near the critical point of the liquid. It was observed that mechanisms of bubble growth in microchannels are much more complicated than in an open environment, which the authors attributed to smaller radius of curvature as predicted by the Young-Laplace equation. The bubbles also differed in having elliptical shapes instead of spherical shapes, as typically results in an open environment.

Bowers and Mudawar (1994a, b) tested heat flux performance of minichannels ( $d = 2.54 \text{ mm}$ ) and microchannels ( $d = 510 \mu\text{m}$ ) with flow boiling of R-113. Heat fluxes in excess of  $200 \text{ W/cm}^2$  were achieved with both low flow rates and low

pressure drops, suitable for electronic cooling. It was observed that for flow boiling a major contributor to pressure drop was the acceleration of the fluid caused by evaporation in the channels. Due to large pressure drops, compressibility effects proved significant for microchannels; however, those effects could be controlled by the combination of lower flow rates and larger channel diameters.

In two-phase cooling, uniformity of device temperature is better achieved with boiling and evaporation where heat transfer to the coolant is mainly latent at the saturation temperature, as opposed to sensible heating in single-phase flow. This phenomenon causes high flux dissipation with very low flow rates; however, vapor production may lead to choking of the flow, causing a large pressure drop in microchannels. Also, transition from nucleate boiling to film boiling causes a drastic drop in heat transfer coefficient resulting in a large rise in surface temperature, an undesirable effect. Considering all these factors and manufacturing ease, Bowers and Mudawar (1994a, b) suggested that minichannels are preferable over microchannels and should be used unless high heat fluxes are required where weight and liquid inventory has to be minimum.

Wang and Beckermann (1993a, b) presented a model for flow and heat transfer of a two-phase mixture. The two phases are regarded as constituents of a binary mixture representing a single material with a smoothly varying phasic composition. Thus the authors avoided using the separate flow model (SFM) where gas and liquid phases are regarded as distinct fluids with individual properties and different flow velocities. This proposed model reduces the differential governing equations by half

when compared with SFM and is applicable to one-dimensional flows with phase change and boundary layer two-phase flows.

Wang and Beckermann (1993a, b) applied their model to analyze two-phase boiling flow along a heated surface embedded in a porous medium. A set of boundary layer equations for two-phase flow was derived and solved by similarity transformation. Although analysis was made for pressure-driven flow, this model can be directly applied to purely buoyancy-driven boiling or condensing flows as well as a combination of both as suggested by the authors.

Chyu and Zaidi (1990) conducted an experimental investigation of pool boiling heat transfer in narrow gaps ranging from 51 to 510  $\mu\text{m}$ . For the same test conditions, local temperature within the gap varied widely due to differences in surface wetting conditions. Hence, the tests were not repeatable. Both heat transfer coefficient and critical heat flux (CHF) could be significantly improved by venting the vapor trapped between the walls.

Xia *et al.* (1992) conducted experiments on boiling heat transfer in narrow channels with gap sizes of 0.8, 1.5, 3.0, 5.0 mm for saturated R-113. Boiling flow pattern and heat transfer were dependent on channel size and heat fluxes. For a particular channel size, there existed a critical heat flux beyond which the heat transfer coefficient decreases rapidly. Results also indicated that channel size could be optimized for an assumed heat flux in which the boiling heat transfer coefficient reaches its maximum.

Orozco and Hanson (1992) studied the effects of surface orientation, liquid temperature, and velocity on nucleate boiling of R-113 from a flat plate in a narrow

channel. They found that in a single-phase convection regime an increase in liquid velocity resulted in a higher heat transfer coefficient, which was not the case in the nucleate boiling regime. Also, a higher heat transfer coefficient was obtained in the convection regime at a higher liquid subcooling. In forced convection, an increase in inclination of the heated plate consistently produced higher heat transfer coefficients. Similar effects were observed with a decrease in channel depth or width. However, since the channel widths varied from 1.59 mm to 25.4 mm similar trends may not be observed in microchannels.

Zhao *et al.* (2000) conducted experimental investigation of flow boiling of CO<sub>2</sub> in microchannels. Heat fluxes ranging from 0.8 to 2.5 W/cm<sup>2</sup> were attained. They also observed that the heat transfer coefficient was independent of heat and mass flux, suggesting other parameters such as size and geometry of the microchannels should be considered. They also performed similar experiments with R-134a as the test fluid. A comparison of the results indicated that heat transfer coefficient for CO<sub>2</sub> was much higher (up to 200%) accompanied by a much lower (60%) pressure drop than that of R-134a. These outstanding heat transfer characteristics of CO<sub>2</sub> were attributed to its thermophysical properties. At 283 K (saturation temperature of the test fluids under experimental condition) the surface tension of CO<sub>2</sub> is 2.67 mN/m which is only one-fourth that of R-134a. Also the viscosity of CO<sub>2</sub> at 283 K is 86.7 μPa.s, only one-third that of R-134a.

Ravigururajan (1998) studied boiling heat transfer and pressure drop characteristics of Refrigerant-124 in rectangular and V-shaped microchannels with hydraulic diameter of 425 μm. It was observed that in subcooled boiling higher heat

transfer coefficient can be attained when inlet subcooling is greater than 8 °C. In the case of saturated flow boiling, heat transfer coefficient varied from high value of 1.8 W/cm<sup>2</sup>-K for a wall superheat of 4 °C to about 0.7 W/cm<sup>2</sup>-K for wall superheat greater than 40 °C. The pressure drop was found to decrease rapidly with an increasing heat transfer coefficient, and increased with an increasing vapor quality.

At this time, the literature contains many results for single-phase flow and few for two-phase or boiling flow in microchannels. Since microfluidics is a new field, enormous opportunities exist to identify new techniques and applications and to conduct theoretical as well as experimental investigations on the fundamentals of fluid flow and heat transfer with and without phase change at the microscale level.

## CHAPTER 3

### THEORY

In this chapter an effort is made to review the conventional flow and heat transfer theory and existing empirical correlations applicable to macrochannel flows. The discussion is limited to rectangular channels only. Due to lack of any established correlation for microscale flow, this review will serve as the basis for comparison with the experimental results of this study. Although the validity of these correlations have not been established for microscale flow, a comparison will certainly provide insight about the effect of microgeometry, if any.

#### Single-Phase Flow

##### Laminar Flow

Darcy friction factor relates wall shear stress to pressure drop in pipes and is defined by the following equation.

$$f = \frac{8\tau_w}{\rho\bar{V}^2} \quad (3.1)$$

where  $\rho$  is density,  $\bar{V}$  is average fluid velocity,  $\tau_w$  is the wall shear stress and is evaluated by using the following relation.

$$\tau_w = -\mu \frac{\partial v}{\partial r} \quad (3.2)$$

where  $v$  represents the local velocity of fluid flowing through a circular pipe,  $\mu$  is the dynamic viscosity and  $r$  represents radial axis. Substitution of the result in the Darcy friction factor equation produces the commonly used laminar Darcy friction factor.

$$f = \frac{64}{\text{Re}} \quad (3.3)$$

The Reynolds number (Re) is defined as

$$\text{Re} = \frac{\rho \bar{V} D}{\mu} \quad (3.4)$$

where  $D$  is the diameter of the pipe. Although the equations above were originally developed for flow through circular pipes, these can be extended to rectangular channels by substituting for the diameter of the pipe by hydraulic diameter  $D_h$ , defined as

$$D_h = \frac{4 \times \text{cross-sectional area } (A_c)}{\text{wetted perimeter } (P)} \quad (3.5)$$

However, a better approximation for fully developed laminar friction factor for rectangular channels can be made by using the following empirical equation by Shah and London (1978):

$$f^* \text{Re} = 96(1 - 1.3553AR + 1.9467AR^2 - 1.7012AR^3 + 0.9564AR^4 - 0.2537AR^5) \quad (3.6)$$

where  $AR$  is the aspect ratio of the rectangular channel (height /width). This equation is accurate to within +0.05% of the analytical values and valid for  $0 \leq AR \leq 1$ .

In forced convection, heat is basically conducted in purely laminar flow since fluid particles remain in streamline. As a result, energy is conducted by those particles as opposed to turbulent flow where fluid particles move across the streamline, thus



exchanging energy in a convective process. Though heat transfer coefficients are considerably smaller in laminar flow than they are in turbulent flow, forced convection laminar heat transfer still has application in mini- and microchannels. For flow through circular tubes, heat and fluid flow correlations can be obtained if the velocity and temperature profiles are known. For laminar, fully developed flow through a circular tube with constant surface temperature, the Nusselt number is constant and given by

$$\text{Nu} = \frac{hD}{k} = 3.657 \quad (3.7)$$

where  $k$  is the thermal conductivity of the fluid, and  $h$  is the heat transfer coefficient. For a similar flow condition as above with constant surface heat flux,  $\text{Nu} = 4.364$ .

Shah and Bhatti (1987) proposed the following correlation that approximates fully developed laminar Nusselt number within  $\pm 0.1\%$  of analytical values for rectangular ducts with prescribed uniform temperature at four walls:

$$\text{Nu}_T = 7.541(1 - 2.61AR + 4.97AR^2 - 5.119AR^3 + 2.702AR^4 - 0.548AR^5) \quad (3.8)$$

Shah and Bhatti (1987) also proposed a similar correlation to approximate Nusselt number within  $\pm 0.03\%$  with uniform heat flux at four walls given by

$$\text{Nu}_H = 8.235(1 - 2.0421AR + 3.0853AR^2 - 2.4765AR^3 + 1.0578AR^4 - 0.1861AR^5) \quad (3.9)$$

Both equations mentioned above are valid for  $0 \leq AR \leq 1$ .

Because the transition flow is very unstable, basic heat transfer and flow friction performances are not yet clearly known.

### **Turbulent Flow**

The first systematic experiment on laminar-to-turbulent transition for flow in a circular pipe was performed by Reynolds. The parameter found to best characterize the laminar and turbulent flow regimes is now recognized as the Reynolds number,  $Re$ . For most practical purposes the flow in the range  $2300 \leq Re < 10,000$  may be regarded as a transition regime for a smooth circular duct, indicating a flow is completely laminar for  $Re \leq 2300$  while it is completely turbulent for  $Re \geq 10,000$ .

The following classical formula by Blasius can determine friction factor for  $4000 \leq Re \leq 10^5$  covering a portion of the transition flow regime and extending to turbulent flow:

$$f = 0.316 Re^{-0.25} \quad (3.10)$$

There are several friction factor correlations for fully developed turbulent flow in a smooth circular duct based on highly accurate experimental results. These results agree quite well among themselves of which the Prandtl-Karman-Nikuradse (PKN) correlation (Bhatti and Shah, 1987) is regarded as the most accurate defined as

$$\frac{2}{\sqrt{f}} = 1.7372 \ln(0.5 Re \sqrt{f}) - 0.3946 \quad 4,000 \leq Re \leq 10^7 \quad (3.11)$$

It is based on the universal velocity distribution law with the coefficients slightly modified to best fit highly accurate experimental data. However, it requires more computational effort due to its implicitness. To avoid this complicity, several explicit correlations are also used to determine friction factor which are extremely

close approximations to the PKN formula. Among them the formula proposed by Colebrook is accurate to within  $\pm 1\%$  of PKN and defined as

$$\frac{2}{\sqrt{f}} = 1.5635 \ln\left(\frac{Re}{7}\right) \quad 4,000 \leq Re \leq 10^7 \quad (3.12)$$

There have been some attempts to develop a single equation to calculate the friction factors for  $2300 < Re < \infty$  spanning the laminar, transition, and turbulent flow regimes. Neither of these analyses produced any simple analytical expressions suitable for engineering computations. The one proposed by Bhatti and Shah (1987) is presented here because of its simplicity and defined as

$$f = A + \frac{B}{Re^m} \quad (3.13)$$

For laminar flow ( $Re < 2100$ ),  $A = 0$ ,  $B = 64$ ,  $m = 1$ ; for transition flow ( $2100 < Re \leq 4,000$ ),  $A = 0.0216$ ,  $B = 9.2 \times 10^{-8}$ ,  $m = -2/3$ , and for transition cum turbulent flow ( $Re > 4,000$ )  $A = 5.12 \times 10^{-3}$ ,  $B = 0.4572$ ,  $m = 3.2154$ . The predictions are in good agreement with the well-established results namely equation (3.3) for laminar flow and the Colebrook equation (3.12) for turbulent flow. Due to its accuracy and simplicity, this correlation will be used to predict friction factor in rectangular microchannels and compared with the experimental results.

For turbulent flow in circular tubes, the simplest heat transfer correlation is given by the Colburn equation (Incropera and DeWitt, 1996) expressed as

$$Nu = 0.023 Re^{0.8} Pr^{1/3} \quad (3.14)$$

where Prandtl number is defined as

$$\text{Pr} = \frac{\mu c_p}{k} \quad (3.15)$$

where  $c_p$  is the specific heat and  $k$  is the thermal conductivity of the fluid. Another classical correlation, the Dittus-Boelter equation (Incropera and DeWitt, 1996) is a slightly different and preferred version of the above result and is of the form

$$\text{Nu} = 0.023 \text{Re}^{0.8} \text{Pr}^n \quad (3.16)$$

where,  $n = 0.4$  for heating and  $0.3$  for cooling. These equations are valid for

$$0.7 \leq \text{Pr} \leq 160$$

$$\text{Re} \geq 10,000$$

$$L/D_h \geq 10$$

These equations are limited to small-to-moderate temperature differences. For flows characterized by large property variations, Seider and Tate recommended the following equation given by Incropera and DeWitt (1996):

$$\text{Nu} = 0.027 \text{Re}^{0.8} \text{Pr}^{1/3} \left( \frac{\mu}{\mu_s} \right)^{0.14} \quad (3.17)$$

$$0.7 \leq \text{Pr} \leq 16,700$$

$$\text{Re} \geq 10,000$$

$$L/D_h \geq 10$$

where  $\mu_s$  is evaluated at the surface temperature of the duct while all other properties are evaluated at mean temperature of the fluid.

For better accuracy a modified correlation proposed by Gnielinski can be used. This equation is given by (Incropera and Dewitt, 1996)

$$\text{Nu} = \frac{(f/8)(\text{Re}-1000)\text{Pr}}{1+12.7(f/8)^{0.5}(\text{Pr}^{2/3}-1)} \quad (3.18)$$

for  $0.5 < \text{Pr} < 2000$  and  $2300 < \text{Re} < 5 \times 10^6$ . This equation can be applied to both uniform surface heat flux and temperature. The experimental results will be compared with the Gnielinski correlation because of its accuracy and also because it covers both the transition and turbulent flow regimes.

However, it should be kept in mind that the correlations proposed above, though highly reliable for macrochannels, may not be so for microchannels. In such cases, the turbulent eddy mechanism for fluid flow and heat transfer is suppressed by the physical size of the channel and may result in lower friction factors and heat transfer coefficients (Bhatti and Shah, 1987).

### **Boiling and Two-Phase Flow**

Heat transfer to boiling liquids is a convection process involving a change in phase from liquid to vapor. The mechanisms of boiling heat transfer are considerably different and more complex than those of single-phase convection. However, this phenomenon has some unique characteristics. Due to the phase change, large heat transfer rates can be achieved without affecting the fluid temperature. While in single-phase convection, the geometry of the system, viscosity, density, thermal conductivity, and specific heat of the fluid are sufficient to describe the process, in boiling heat transfer the surface characteristics, surface tension, latent heat of evaporation, pressure, and buoyancy force play an important role.

When evaporation occurs at a solid-liquid interface, the phenomenon is called boiling, and it takes place when the surface temperature  $T_s$  exceeds the saturation

temperature  $T_{\text{sat}}$  of the liquid. The process is characterized by formation of vapor bubbles, the dynamics of which affect fluid motion near the surface, thus influencing the heat transfer coefficient.

Boiling may be classified according to the conditions under which it occurs. In pool boiling, liquid motion near the surface is due to free convection and mixing induced by bubble growth and detachment, while in forced convection, boiling fluid motion is induced by external means together with free convection and bubble-induced mixing.

### **Pool Boiling**

In saturated pool boiling, bubbles generated at the liquid-solid interface are transported across the liquid-vapor interface by buoyancy forces and eventually escape from the free surface. The fundamental mechanisms of pool boiling can be better understood by examining the different boiling regimes as represented by the following boiling curve.

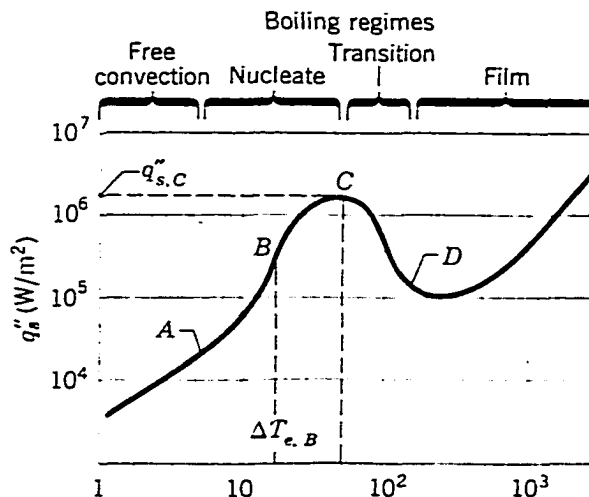


Figure. 3.1: Boiling curve of water (Incropera and DeWitt, 1990)

$\Delta T_E$  is the excess temperature above saturation temperature. For  $\Delta T_E < 5^\circ\text{C}$ , free convection boiling occurs and fluid motion is governed by free convection effects. Bubble inception does not occur until point A is reached, a term referring to the onset of nucleate boiling.

Nucleate boiling exists from point A to point C. In this regime, the heat flux continues to increase till it reaches a critical value,  $q''_{\max}$  at C. The heat transfer coefficient  $h$  begins to increase from A, reaches its maximum at B, the inflection point, and then begins to decrease. However, Tong *et al.* (1997) suggested that the amount of heat transferred by latent heat transport of bubbles is usually small in comparison with the convective component. Based on the experimental findings of other researchers, he suggested that intense agitation of the liquid layer close to the surface (termed microconvection) is the reason for high heat transfer rate in boiling. Another hypothesis assumes the vaporization of a microlayer of liquid underneath a bubble, since experimental work indicates that during nucleate boiling of water at atmospheric pressure surface temperature occasionally drops  $10^\circ\text{C}$  to  $15^\circ\text{C}$  in about 2 milliseconds. This hypothesis was verified by calculations and also by optical techniques.

Due to the high heat transfer rates and convection coefficients, it is of great engineering interest to set the operating condition of most heat exchangers in the nucleate boiling regime. In this region, the critical heat flux (CHF) is given by (Incropera and DeWitt, 1990)

$$q_{\max} = 0.149 h_{fg} \rho_v \left[ \frac{\sigma g (\rho_l - \rho_v)}{\rho_v^2} \right]^{1/4} \quad (3.19)$$

Using bubble diameter  $d_b$  as the characteristic length for nucleate boiling, the Nusselt number may be defined as

$$Nu_b = h_b d_b / k_f \quad (3.20)$$

where  $h_b$  is the nucleate boiling heat transfer coefficient defined as (Kreith, 1970)

$$h_b = (q/A) / \Delta T_E \quad (3.21)$$

Critical heat flux depends strongly on pressure, surface tension and latent heat of evaporation. If the heat flux is controlled, any increase in  $q_s''$  beyond point C will force the boiling point to shift from point C to point E, which may result in failure of the system due to an abrupt increase in temperature, a phenomenon often termed 'boiling crisis'. For this reason, accurate knowledge of the critical heat flux is important to determine the safe operating temperature of any device.

In the transition boiling region, bubble formation is so rapid that a vapor film forms on the surface. The boiling condition oscillates between film and nucleate boiling and both  $h$  and  $q_s''$  decrease with increasing  $\Delta T_E$ . Later in film boiling, radiation through the vapor film becomes dominant rather than convection and heat flux increases with increasing  $\Delta T$ .

Considering the characteristics of different regimes, it is obvious that the maximum consideration should be given to nucleate boiling. Also, due to pressure driven flow under consideration, forced convection boiling and associated correlations need to be considered.

Ordinarily two-phase flow with heat addition is a coupled thermodynamic problem. On one side, heat transfer causes phase change and hence a change of phase



distribution and flow pattern; on the other side, a change in the hydrodynamics, caused by pressure drop along the flow path, affects the heat transfer characteristics. A single component two-phase flow can never become fully developed. The inherent pressure change along the channel continually changes the state of the fluid and thus changes the phase distribution and flow pattern (Tong *et al.* 1997).

Due to the complexities mentioned above, simplified analytical and experimental studies have been conducted, often based on the assumptions of fully developed flow patterns and without heat addition to the flow. Thus, the information available on flow patterns, phase distribution, and pressure drop in adiabatic flows are often based on two-component gas-liquid mixtures. Based on visualization studies, a generally accepted classification of typical flow regimes for two-phase two-component flows are depicted in Figure 3.2. A description is given below in the order of increasing quality from single-phase liquid flow to single-phase vapor flow.

1. **Bubble Flow:** in this regime, the liquid phase is continuous and the vapor phase is discontinuous. The vapor is distributed in the liquid in the form of bubbles and tend to flow at or near the upper surface of the channel.
2. **Plug Flow:** Here the bubbles are large enough to occupy the upper surface of the channel, though the vapor phase is still discontinuous. This is only a transitory stage to the next regime.
3. **Stratified Flow:** In this regime, the gas and liquid flow as separate entities and both are continuous. The flow rates are independent of each other.

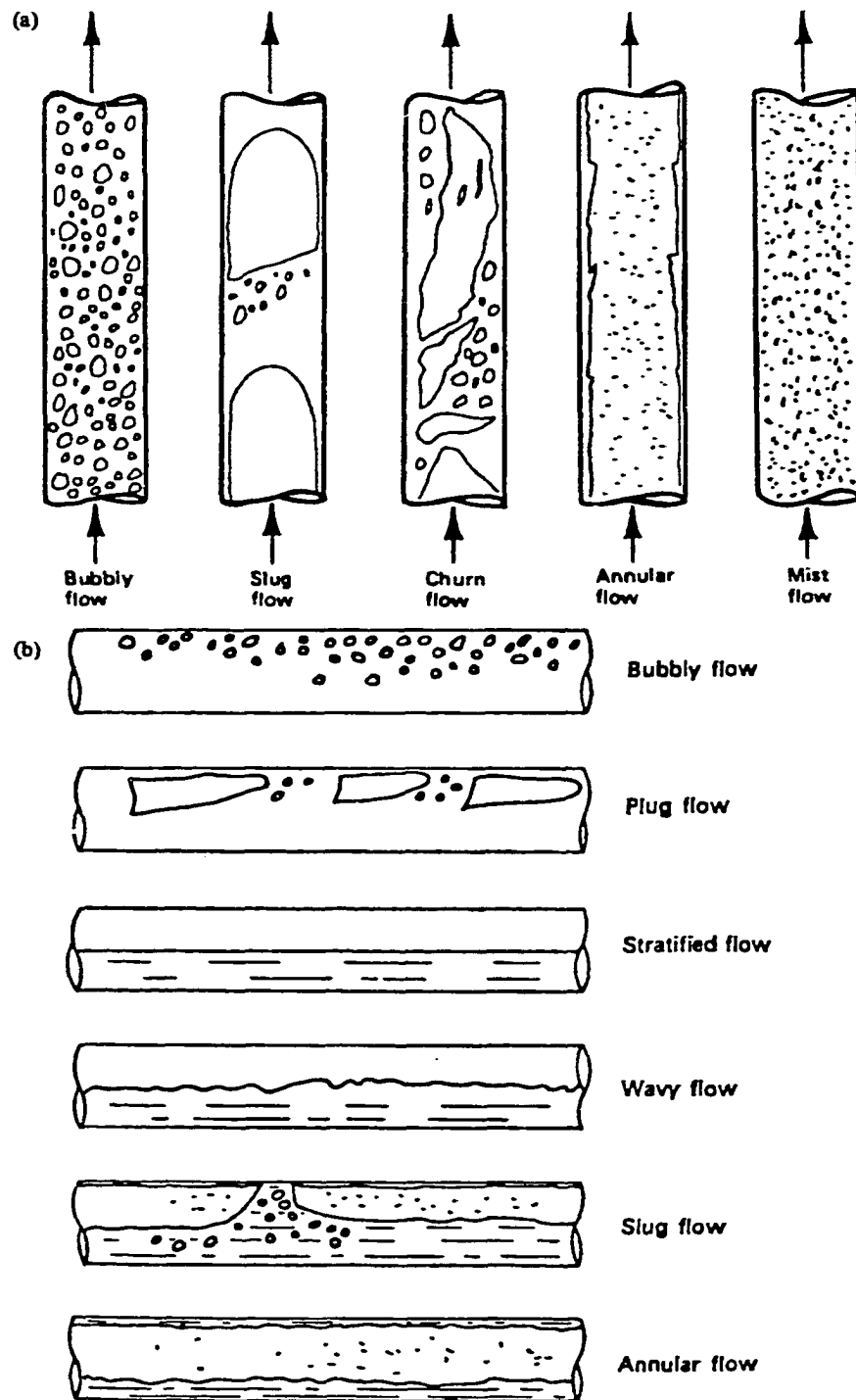


Figure 3.2: Flow regimes in a two-phase flow (Tong *et al.*, 1997)

4. Wave Flow: the gas flow rate is quite large compared to the liquid flow rate and produces wave in the liquid. The next regime begins when the liquid waves reach the top surface of the channel.
5. Slug Flow: in this regime, relatively large liquid slugs appear in the flow as a result of agglomeration of vapor bubbles. Slugs of liquid and bubbles follow each other and can cause instabilities in the flow due to the sectional differences in density and compressibility. This flow occurs at relatively low flow velocities. This type of flow does not develop at a high heat flux or in a short channel.
6. Annular Flow: in this regime, the liquid phase is continuous in an annulus along the wall and vapor phase is continuous in the core. Discontinuous liquid phase is present in the core as droplets, while discontinuous vapor phase appears as bubbles in annulus. This pattern occurs at high flow velocities. A special case of annular flow is that in which a vapor film is along the wall, and a liquid core is in the center. This type of flow occurs only in subcooled stable film boiling.
7. Mist Flow: this flow regime has the same characteristic of having a liquid film as an annulus along the surface, only much thinner than annular flow. This liquid annulus keeps on decreasing until only vapor flows through the channel.

### **Flow Boiling**

Flow boiling is distinguished from pool boiling by the presence of fluid flow caused by natural circulation in a loop or forced by an external pump. However, at steady state the flow appears to be forced in both cases. When the heat flux from the heating surfaces is increased above a certain value, the convective heat transfer is not

enough to prevent the wall temperature from rising above the saturation temperature of the fluid. This elevated wall temperature superheats the liquid in contact with the wall and activates nucleation sites, generating bubbles. Initially nucleation occurs only in patches along the heated surface. This regime is termed partial nucleate boiling. As the heat flux is increased, more nucleation sites are activated until at fully developed nucleate boiling all surfaces are in nucleate boiling. The process continues until critical heat flux is reached same as in pool boiling. Beyond critical heat flux, the heat transfer is unstable and termed transition boiling. Transition boiling is gradually converted to stable film boiling as the surface temperature increases above the Leidenfrost point.

As in pool boiling, the flow boiling crisis is characterized by a sudden drop in the heat transfer coefficient due to change of boiling mechanisms and is indicated by a temperature rise of the heated surface. However, the mechanism is different from that in pool boiling. In addition to the forced convection effect of the flow, it is further complicated by two phenomena that strongly affect the critical heat flux which are described below.

1. Bubble clouding: in flow boiling, often a layer of bubbles is moving parallel to the heated surface. This layer shields the surface from incoming cold liquid.
2. Flow instability: the boundary layer is retarded periodically by the changing flow velocity. The heated surface under this temporary stagnant layer may become overheated, resulting in a premature boiling crisis. Another reason could be the temporary lowering of the local pressure, increases the local superheat near the wall temporarily. This superheat produces more bubbles destroying the liquid film.

Flow boiling crisis is closely related to the type of flow pattern present at its occurrence. So, based on flow conditions, the flow boiling crisis can be classified into following two categories.

1. Boiling crisis in a subcooled or low quality region: this type occurs only at high heat flux, at a high flow rate. The fluid near the surface may not be in a thermodynamic equilibrium with the bulk stream. The high heat flux causes an intensive boiling, making the bubbles agglomerate near the heated surface. These bubbles impair the surface cooling by reducing the amount of incoming liquid. The high heat flux causes the surface temperature to rise rapidly and may result in physical burnout. Hence, this type of boiling crisis is often called fast burnout.
2. Boiling crisis in a high-quality region: this type of boiling crisis occurs at a lower heat flux than the previous case. The total mass flow rate could be small and the flow pattern is generally annular. In this case, usually a liquid layer normally covers the heated surface and acts as a cooling medium. If this layer breaks down due to excessive evaporation, a boiling crisis will occur. The surface temperature will rise, but due to good heat transfer coefficient of a fast-moving vapor core it is usually slower than that in a subcooled boiling crisis. This situation is often termed as slow burnout.

Different flow regimes were investigated by researchers for both horizontal and vertical flows using air and water. Baker (1954) looked at data from a variety of sources and came up with a flow regime map that has long been considered a representative plot for horizontal flow. The plot was later modified by Scott (Tong *et al.* 1997) and is shown in Figure 3.3. The parameters used are  $G/\lambda$  and  $\lambda\psi L/G$ , where

$G$  and  $L$  are the vapor and liquid mass flux, respectively, based on total cross-sectional area of the pipe and

$$\lambda = \left[ \left( \frac{\rho_G}{\rho_{\text{air}}} \right) \left( \frac{\rho_L}{\rho_{\text{water}}} \right) \right]^{1/2} \quad (3.22)$$

$$\psi = \left( \frac{\sigma_{\text{water}}}{\sigma} \right) \left[ \mu_L \left( \frac{\rho_{\text{water}}}{\rho_L} \right) \right]^{2/3} \quad (3.23)$$

where the subscripts refer to the particular vapor ( $G$ ) and the particular liquid ( $L$ ). These factors are used primarily for the translation from mostly air-water data to other gas-oil systems. The values of the properties of the air and water are taken at standard atmospheric conditions.

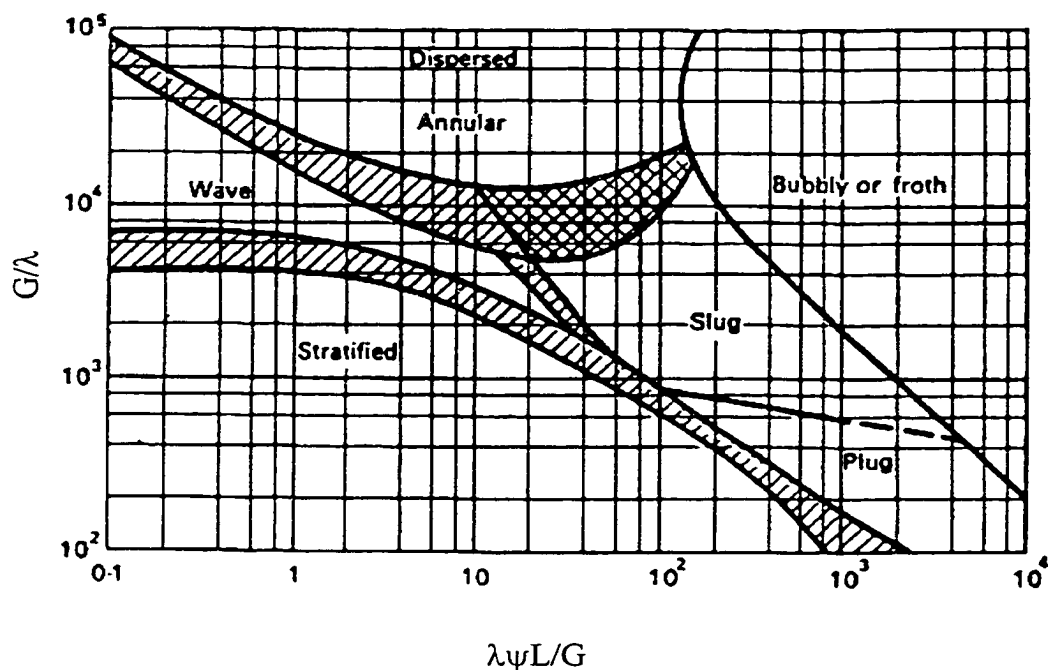


Figure 3.3: Flow Regime Map for horizontal flow (Tong *et al.* 1997)

## CHAPTER 4

### EXPERIMENTAL SET-UP AND PROCEDURE

This chapter gives an overview of the experimental apparatus used to conduct the experiment. It also includes a detailed description of the procedures followed to perform the experiment. Later, data reduction technique and an error analysis of the results are presented using a sample data.

#### Experimental Apparatus

##### Test Section

The test section configuration was originally designed by Bailey (1996) to determine friction factor in microchannel flow; this configuration was later modified by Stanley (1997) to incorporate heat transfer experiments. The same test section was used for this study. The test section (Figure 4.1) consisted of an aluminum blank in which the microchannels were machined, sealed by a glass cover plate (not shown).

The microchannels were fabricated from 0.3175 cm (0.125 in) thick 6061-T6 aluminum bars. Aluminum was chosen because of its high thermal conductivity and also because it can be machined easily. Conventional cutting and milling processes were used to machine the aluminum blanks to 2.54 cm x 10.16 cm (1 in x 4 in) size. A Computer Numeric Control (CNC) program written by Bailey (1996) was used to fabricate the blanks uniformly. Both the manifold and the glue channels were cut to a

depth of 0.3175 cm (0.0625 in). Two holes of diameter 0.635 cm (0.25 in) were drilled through the blank to allow the fluid to enter into and leave from the manifold. The design allowed a maximum length for the microchannels to be 6.35 cm (2.5 in). This length ensured that most of the flow in the channels was fully developed. The channels ranged from approximately 210  $\mu\text{m}$  to 112  $\mu\text{m}$  in hydraulic diameter. These were machined using the Ultra Precision Milling Machine by Dover Instrument Corporation at Institute for Micromanufacturing of Louisiana Tech University. Micro end-mills from McMaster-Carr and Mini Tool Inc., were used to cut the channels. A detailed description of the processes involved, including surface finish and metrology of the microchannels is provided by Bailey (1996). Table 1 lists the measured channel parameters for each configuration. Among the four configurations used, three had an aspect ratio of approximately one. However, for configuration C2 aspect ratio was about 1.5. It was done to consider the effect of geometry, if any. The channel dimensions and surface characteristics were measured by using a WYKO Roughness /Step Tester (RST). The widths of the channels were measured using a microscope /video camera system with a frame grabber software. The system was calibrated using micromasurement slides from Edmund Scientific. Finally, the channel length was determined by using a Max Cal digital dial caliper with an accuracy up to 0.001 cm (0.0005 in). The accuracy of all these measurements is discussed in the Error Analysis section later this chapter.



Table 4.1: Measured Microchannel Dimensions

Channel Designation	Avg. Roughness, nm	Avg. Depth, $\mu\text{m}$	Avg. Width, $\mu\text{m}$	Aspect Ratio	Hydraulic Diameter, $\mu\text{m}$	Number of Channels
B	1547.1	211.1	208.9	1.01	210.1	3
C1	290.4	134.6	121.8	1.105	127.9	5
C2	1846.2	263.73	170.4	1.548	207.01	3
D	183.9	111.3	112.4	1.01	111.9	7

The test sections were covered with a glass plate using epoxy. However, since the glass plates were not perfectly flat, a Loctite-UV cure adhesive (Product 3336) was used to ensure proper sealing. The UV adhesive was thinned with acetone and the mixture was poured on the polished side of a clean 4 inch silicon wafer. As the acetone was allowed to evaporate (approximately 90 seconds) under UV lamp, a thin layer of adhesive was formed on the wafer. The thin layer of adhesive was removed, and the side exposed to the atmosphere was attached to the top surface of the aluminum blank. Care was taken to completely cover the channels and the manifold areas. A thin layer of transparent epoxy was spread over the cover plate and was hand-pressed against the adhesive layer on aluminum blank to ensure proper contact between the surfaces. Then the combination was taped and left in room temperature for approximately 3 days to cure the epoxy. The epoxy was chosen such that it will not soften at the operating temperature of the experiment and at the same time softening point low enough to be melted in order to remove the cover without damaging the thermocouples. It is important not to use the same UV adhesive to bond the cover plate. The uncured adhesive would slightly dissolve the cured adhesive causing the

channels to be clogged. The assembly was allowed to dry without using any pressure. Any pressure could push the partially cured adhesive into the channels to clog them. When the epoxy was completely cured, the channel blank was placed in an oven set at 65 °C (150°F) for approximately 14 hours. This was done to cure the UV adhesive completely. The thermocouples were installed in the backside of the blank before the channels were sealed.

Figure 4.1 also shows the location of the seven small thermocouples placed underneath the microchannels. The thermocouples were type-T (copper-constantan) and were fabricated from 36-gauge wire coated with Teflon. Small grooves were machined on the back side of the blank to accommodate the thermocouple wires. The wires were glued using a high-temperature, high thermal conductivity epoxy to minimize heat loss due to the glue. It should be noted that three thermocouples numbered 3, 4, and 5 were located in a lateral direction to check for any lateral heat conduction that might be present across the blank, which would be indicated by unequal readings of those thermocouples. The distance from the microchannel wall to the thermocouple was chosen so that an assumption of a constant wall temperature between the wall and the thermocouple could be made. The thermal conductivity of 6061-T6 aluminum at 300 K is approximately 177 W/m-K. In this study the maximum heat dissipated was about 67.5 W and the smallest area was for channel D with seven 112 μm wide channels. The center-to-center distance of the channels were about five channel widths. From Fourier law of conduction

$$q = kA \frac{dT}{dx} \approx kA \frac{\Delta T}{\Delta x} \quad (4.1)$$

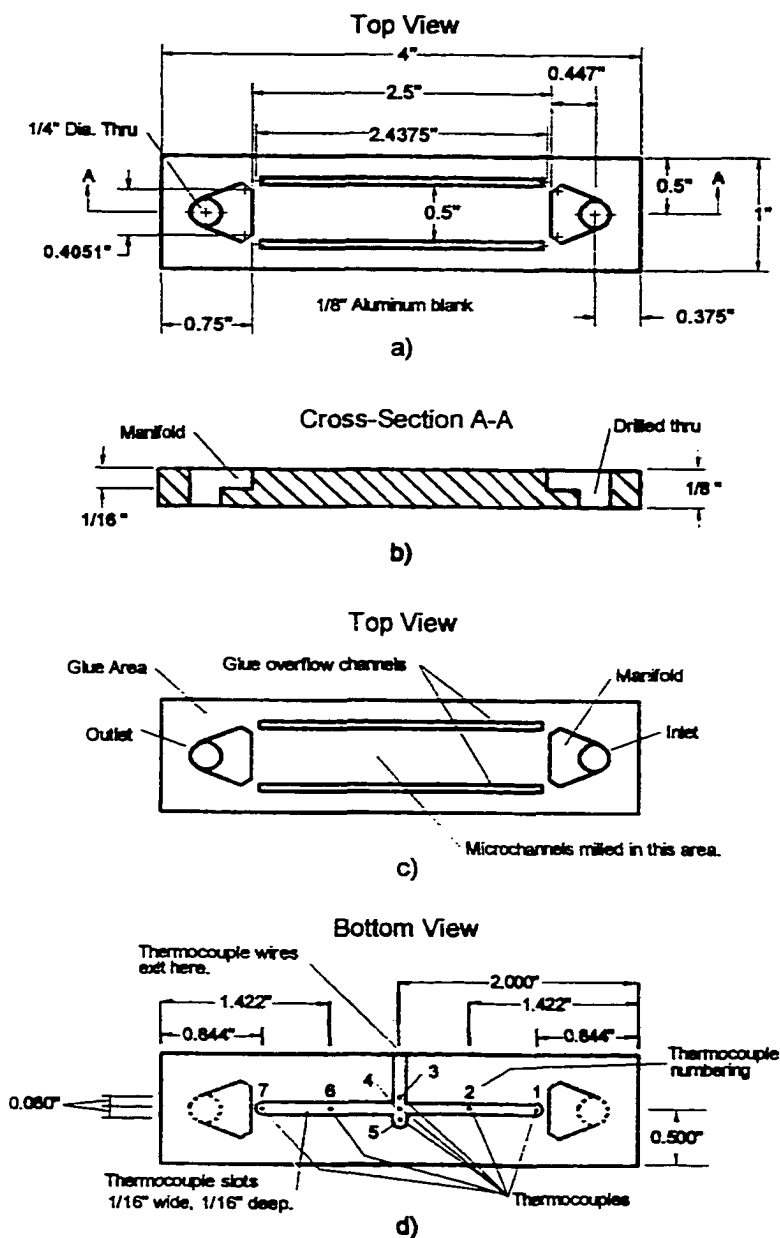


Figure 4.1: Test Section; (a) Dimensions, (b) Cross-section, (c) Component description, and (d) Thermocouple locations and numbering, approximately 0.01" beneath channels

Solving for  $\Delta T$ , one gets

$$\Delta T = \frac{q \Delta x}{kA} \quad (4.2)$$

For  $\Delta x = 0.01$  inch (0.25 mm) and a channel length of 2.5 inches (0.0635 m)

$$\Delta T = \frac{(67.5 \text{ W})(2.54 \times 10^{-4} \text{ m})}{(177 \text{ W/m-K})\{7 \times 5 + 1\}(112 \times 10^{-6} \text{ m})(6.35 \times 10^{-2} \text{ m})} = 0.38^\circ \text{C} \quad (4.3)$$

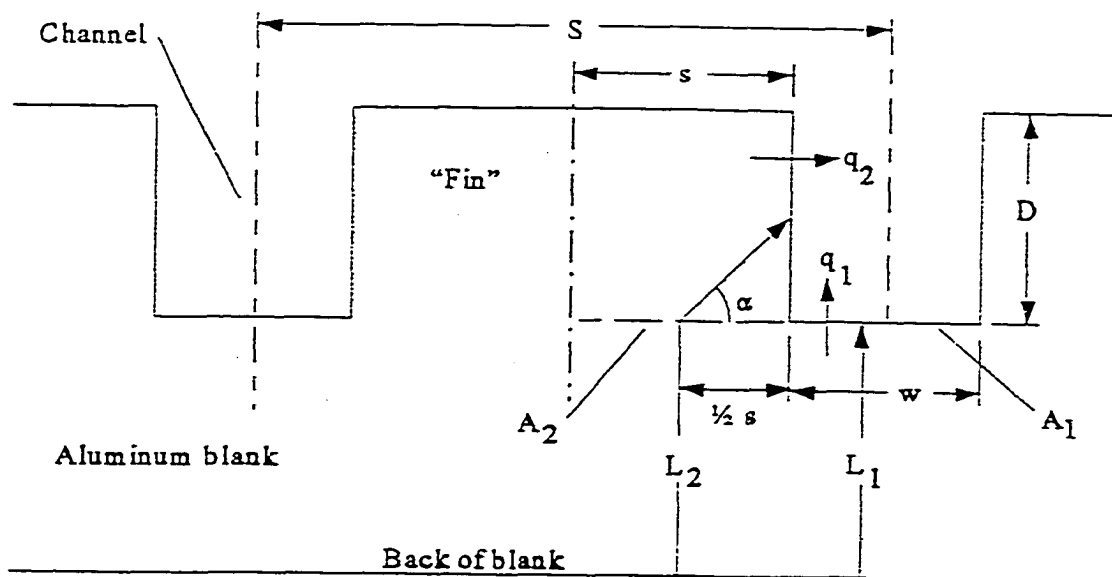
The accuracy of the thermocouples is  $\pm 1.0^\circ \text{C}$ . This result validates the assumption that the temperature readings from thermocouples are essentially same as channel walls, since the temperature variation within the aluminum wall is too small to be measured accurately.

The mathematical model of determining the center-to-center distance of the channels was reported by Stanley (1997). All the variables used in this modeling are defined in Figure 4.2. It is assumed that equal amount of heat are transferred to both area one and area two. In mathematical form

$$q_1 = q_2 \quad (4.4)$$

$$\frac{k_1 A_1 \Delta T_1}{L_1} = \frac{k_2 A_2 \Delta T_2}{L_2} \quad (4.5)$$

For a homogeneous solid blank,  $k_1 = k_2$ . As shown previously, wall temperature can be assumed to be constant for all practical purposes and hence  $\Delta T_1 = \Delta T_2$ . Defining  $A_1 = wl$ ,  $A_2 = sl$ , and  $L_2 = L_1 + D/(2 \sin 45^\circ)$ . The angle of  $\alpha = 45^\circ$  is assumed and will be compared with the theoretically calculated value. Plugging in these variables in Equation (4.5) yields



Definition of variables:

$D$  = depth of channel

$w$  = width of channel

$s$  =  $\frac{1}{2}$  distance between edge of adjacent channels

$S = 2s + w$

$A_1$  = heat transfer area for lower surface of channel

$A_2$  = horizontal heat transfer area for  $\frac{1}{2}$  width of "Fin"

$L_1$  = thickness from back of blank to lower surface of channel

$L_2$  = distance from back of blank to center of side wall through angle  $\alpha$

$l$  = length of the channel

$q_1$  = heat transfer through lower surface of channel

$q_2$  = heat transfer through side wall of channel

Figure 4.2: Mathematical model to determine channel spacing

$$sl = w \left[ \frac{L_1 + \frac{D}{2 \sin 45^\circ}}{L_1} \right] \quad (4.6)$$

Simplification results in the final expression

$$s = w \left( 1 + \frac{D}{2 L_1 \sin 45^\circ} \right) \quad (4.7)$$

Assuming the area between the channels behaves as a fin, the channel configuration C2 with the largest aspect ratio presented the worst case in this study. The expected dimensions of channel C2 were  $170 \mu\text{m} \times 263 \mu\text{m}$ . For the aluminum blank  $L_1 \approx 2,912 \mu\text{m}$ . Substitution of these values in equation (4.7) yields

$$s = (170 \times 10^{-6} \text{ m}) \left( 1 + \frac{263 \times 10^{-6} \text{ m}}{2 (2912 \times 10^{-6} \text{ m}) \sin 45^\circ} \right) = 180.86 \times 10^{-6} \text{ m} \quad (4.8)$$

In terms of channel width it can be expressed as,

$$s = \frac{181}{170} w = 1.06 w \quad (4.9)$$

Rounding up the number to  $s = 1.5 w$  and defining the center-to-center distance between the channels as

$$S = 2s + w \quad (4.10)$$

Substituting in the above expressions for  $s$  gives

$$S = 2 (1.5 w)s + w = 4w \quad (4.11)$$

Allowing a factor of safety, the channel spacing was set at

$$S = 5w \quad (4.12)$$

Thus the center-to center distance of the channels is equal to five widths of the channel. For configuration C2, the assumed angle of  $\alpha = 45^\circ$  can be checked from these findings. For channel C2,  $D = 263.7 \mu\text{m}$ ,  $S = 5(127 \mu\text{m}) = 635 \mu\text{m}$ , and  $s = (S - 127 \mu\text{m})/2 = 254 \mu\text{m}$ . Then,

$$\alpha = \tan^{-1}\left(\frac{D}{s}\right) = \tan^{-1}\left(\frac{263.7}{254}\right) = 46.1^\circ \quad (4.13)$$

Therefore, the assumption of  $\alpha = 45^\circ$  can be considered reasonable.

The validity of the previously described channel spacing can be determined using the theory of heat conduction through fins. Two assumptions are made in this analysis; these are (1) a constant wall temperature and (2) equal heat fluxes from the walls of a channel. From the fin theory, the temperature distribution in a fin with adiabatic tip is given by (Incropera and DeWitt, 1996)

$$\frac{\theta}{\theta_b} = \frac{\cosh m(L - x)}{\cosh mL} \quad (4.14)$$

where  $\theta = T_{\text{fin}} - T_\alpha$ ,  $\theta_b = T_{\text{wall}} - T_\alpha$ ,  $m^2 = hP/kA_c$ ,  $L = \text{fin height (channel depth)}$ ,  $x = 0 \rightarrow L$  from base of fin,  $h = \text{heat transfer coefficient}$ ,  $k = \text{thermal conductivity of fin material (aluminum blank)}$ ,  $\text{fin perimeter } P = 2w + 2t$ ,  $A_c = wt$  (cross-sectional area of fin),  $w = \text{fin width (channel length)}$ , and  $t = \text{fin thickness (distance between edges of two channels)}$ . For configuration C2, based on experimental data the maximum values of  $h$  and  $\theta$  were found to be  $9,600 \text{ w/m}^2\text{-K}$  and  $20^\circ\text{C}$  respectively. Also  $L = 263.7 \mu\text{m}$ ,  $t = 4 \times 170.4 \mu\text{m} = 681.6 \mu\text{m}$  and  $w = 0.0635 \text{ m}$ . Substitution of these values into the definitions yields

$$P = 2(0.0635 \text{ m}) + 2(681.6 \times 10^{-6} \text{ m}) = 0.128363 \text{ m}$$

$$A_c = 0.0635 \text{ m} \times 681.6 \times 10^{-6} \text{ m} = 4.32816 \times 10^{-5} \text{ m}^2$$

$$m = \left\{ \frac{(9,600 \text{ W/m}^2 - K)(0.128363 \text{ m})}{(177 \text{ W/m-K})(4.32816 \times 10^{-5} \text{ m}^2)} \right\}^{1/2} = 401.067 \text{ m}^{-1} \quad (4.15)$$

$$mL = 401.067 \text{ m}^{-1} \times 263.7 \times 10^{-6} \text{ m} = 0.10576$$

The largest temperature difference should occur between the base and fin tip. So the temperature distribution of the fin from equation (4.13) at  $x = L$  would be

$$\frac{\theta}{\theta_b} = \frac{\cosh(0)}{\cosh(0.10576)} = 0.994433 \quad (4.16)$$

For  $\theta_b = 20 \text{ }^\circ\text{C}$ ,  $\theta = 19.88 \text{ }^\circ\text{C}$ . Thus the maximum temperature drop within the fin was  $20 - 19.88 = 0.12 \text{ }^\circ\text{C}$ . Since the thermocouples have an accuracy of  $\pm 1.0 \text{ }^\circ\text{C}$ , the temperature drop across the fin was too small to be measured accurately. This result justifies the assumption of constant wall temperature.

The constant heat flux assumption was examined by calculating the heat flux for a given fin and then comparing it with the heat loss through the channel bottom. For an adiabatic tip fin, the heat transfer rate is given by (Incropera and DeWitt, 1996)

$$q_f = \sqrt{hPkA_c} \theta_b \tanh mL \quad (4.17)$$

where all the parameters have been defined previously. By defining  $M = (hPkA_c)^{0.5} \theta_b$ , and plugging in the values,

$$M = [(9,600 \text{ W/m}^2 - K)(0.128363 \text{ m})(177 \text{ W/m-K})(4.32816 \times 10^{-5} \text{ m}^2)]^{1/2} (10 \text{ }^\circ\text{K})$$

$$M = 61.45 \text{ W}$$

and substituting these values in equation (4.17)

$$q_f = (61.45 \text{ W}) \tanh(0.10576) = 6.47 \text{ W} \quad (4.18)$$

For similar conditions the heat loss through the bottom of the channel is given by



$$q_b = hA_b(T_b - T_\alpha) \quad (4.19)$$

$$q_b = (9,600 \text{ W/m}^2\text{-K})(1.704 \times 10^{-4} \text{ m})(0.0635 \text{ m})(20 \text{ }^\circ\text{K}) = 2.0775 \text{ W}$$

where  $A_b$  is the cross-sectional area of the bottom wall. However, since channel C2 has an aspect ratio of 1.548, the fin wall area is actually  $2 \times 1.548 = 3.096$  times larger than the area of the bottom wall taking both sides of the fin into consideration. So the maximum heat loss that occurred through each wall compared with the bottom wall would be

$$\frac{2.0775 - \frac{6.47}{3.096}}{2.0775} = 0.006 = 0.6\% \quad (4.20)$$

Considering thermocouple accuracy and experimental uncertainties a 0.6% fluctuation in heat flux can be considered reasonable to make a constant heat flux assumption.

### **Test Fixture**

The test fixture holds the test section in place and is shown in Figure 4.3. Arrangements were made to measure temperatures and pressures at the inlet and outlet of the test section. In addition, it houses an OMEGA (1 inch x 2.5 inch) Kapton heater, which provides the heat flux required for heat transfer analysis. The heater was rated at 121 ohms with a maximum heat flux of 6 Watts. The heater was mounted in between a piece of silicon wafer and a high-temperature epoxy /fiberglass material. The silicon wafer helped to evenly distribute the heat over the test section while the epoxy /fiberglass material provided rigidity and a means to mount the heater thermocouple without actually touching the heater. Teflon was used underneath the heater to provide high-temperature thermal insulation, and the entire test fixture was

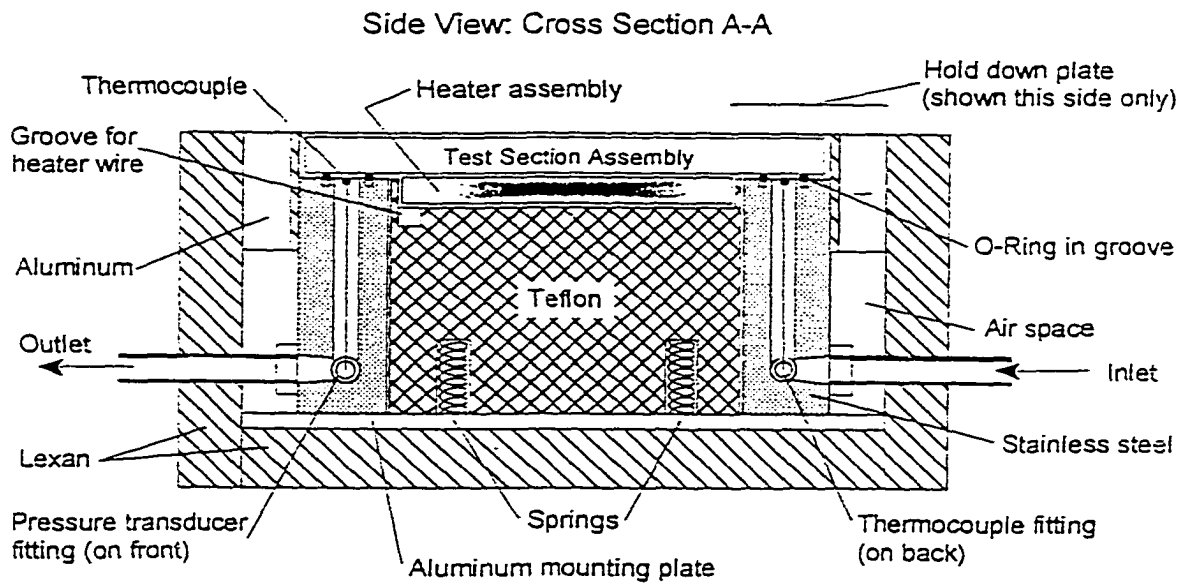
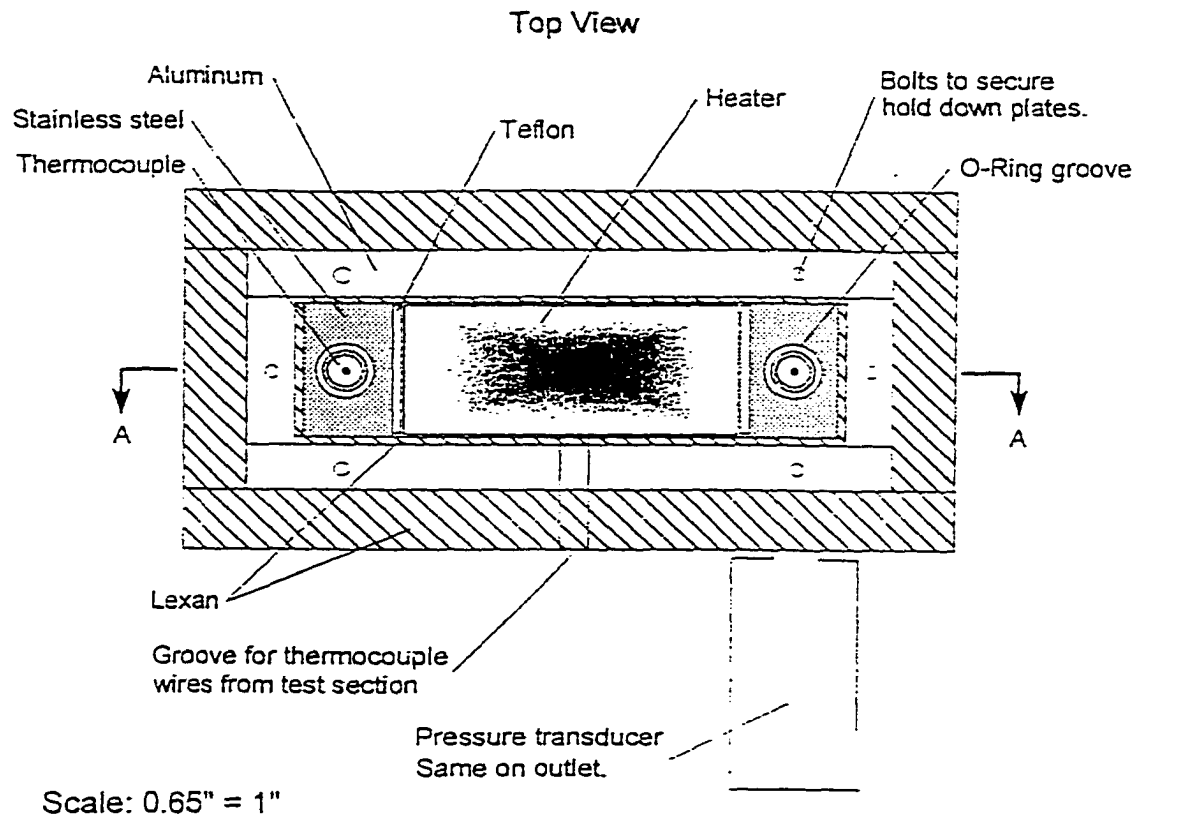


Figure 4.3: Test fixture assembly.

insulated from its surroundings using Lexan (polycarbonate). Two different insulating materials were used because Teflon has a higher melting point, making it suitable for heater insulation, while Lexan has better insulating properties and machinability. It was done to prevent any contact between the channel blank and its surrounding aluminum body, which would conduct heat affecting the experimental results.

The channel blank rested on an O-ring mounted in the manifold. These O-rings were made of ethylene propylene (EPDM). EPDM was chosen for its resistance to corrosion against refrigerants. Care was taken not to overcompress the O-rings as the test section was placed because this action would allow the test section to come in contact with the surrounding metal part of the fixture. On the other hand, undercompressed O-rings could blow out of their grooves due to high inlet pressure. Selected thermal and mechanical properties of the materials used in fabricating the test section, test fixture, and flow loop are presented in Table 4.2.

Table 4.2: Thermal and Mechanical Properties of Experimental Apparatus Materials

Material	Thermal Conductivity (k) W/m-K	Thermal Expansion ( $\alpha$ ) $1/^\circ\text{C}$	Melting Point ( $^\circ\text{C}$ )	Yield Tensile Strength MPa (psi)
Teflon	0.25	$1 \times 10^{-4}$	> 287	17 – 31 (2,500 – 4,500)
Lexan	0.19	$8 \times 10^{-5}$	148	55 – 62 (8,000 – 9,000)
EPDM			150 (softening temp.)	
Glass	1.08	$80 \times 10^{-6}$	820	
Aluminum	177	$23.6 \times 10^{-6}$	527	255 (37,000)
Stainless Steel	14.7	$17.3 \times 10^{-6}$	1,400	520 (75,000)
Omegatherm 201	2.3		200	

## **Flow Loop**

The flow loop was designed to conduct microscale fluid flow and heat transfer experiments for a variety of fluids and flow conditions. A schematic of the flow loop is given in Figure 4.4. A complete description of the apparatus can be found in Bailey (1996). Figures 4.5 and 4.6 show the general layout of the flow loop. The wetted parts of the flow loop were constructed almost entirely of stainless steel with EPDM seals to make the whole system corrosion resistant and also to be able to handle broadest range of fluids, flow rates, temperatures, and pressures.

The reservoir was fabricated from stainless steel with a limiting pressure of approximately 2,000 kPa (300 psig). However, the tank design pressure should not be reached since the flow-loop pump had a limitation of 1380 kPa (200 psig) on the back pressure. A safety relief valve was mounted on the reservoir to maintain within a safe limit the pressure inside the reservoir. It was used as a pressure vessel to keep the refrigerant in liquid form at room temperature. However, it could also be used as an open tank for fluids (e.g., water) where no back pressure was required. The temperature of the fluid in the reservoir could be controlled by using a constant temperature water bath to circulate water through a coiled stainless steel tubing inside the reservoir.

It was determined that a low flow rate pump with flexibility in range and minimum pulsation in flow could be used for this research. However, because the refrigerant was always maintained at a high pressure, the pump had to be able to handle a high inlet pressure as well which restricted our choice to gear pumps only. Accordingly, an adjustable-speed gear pump with back pressures up to 1380 kPa (200

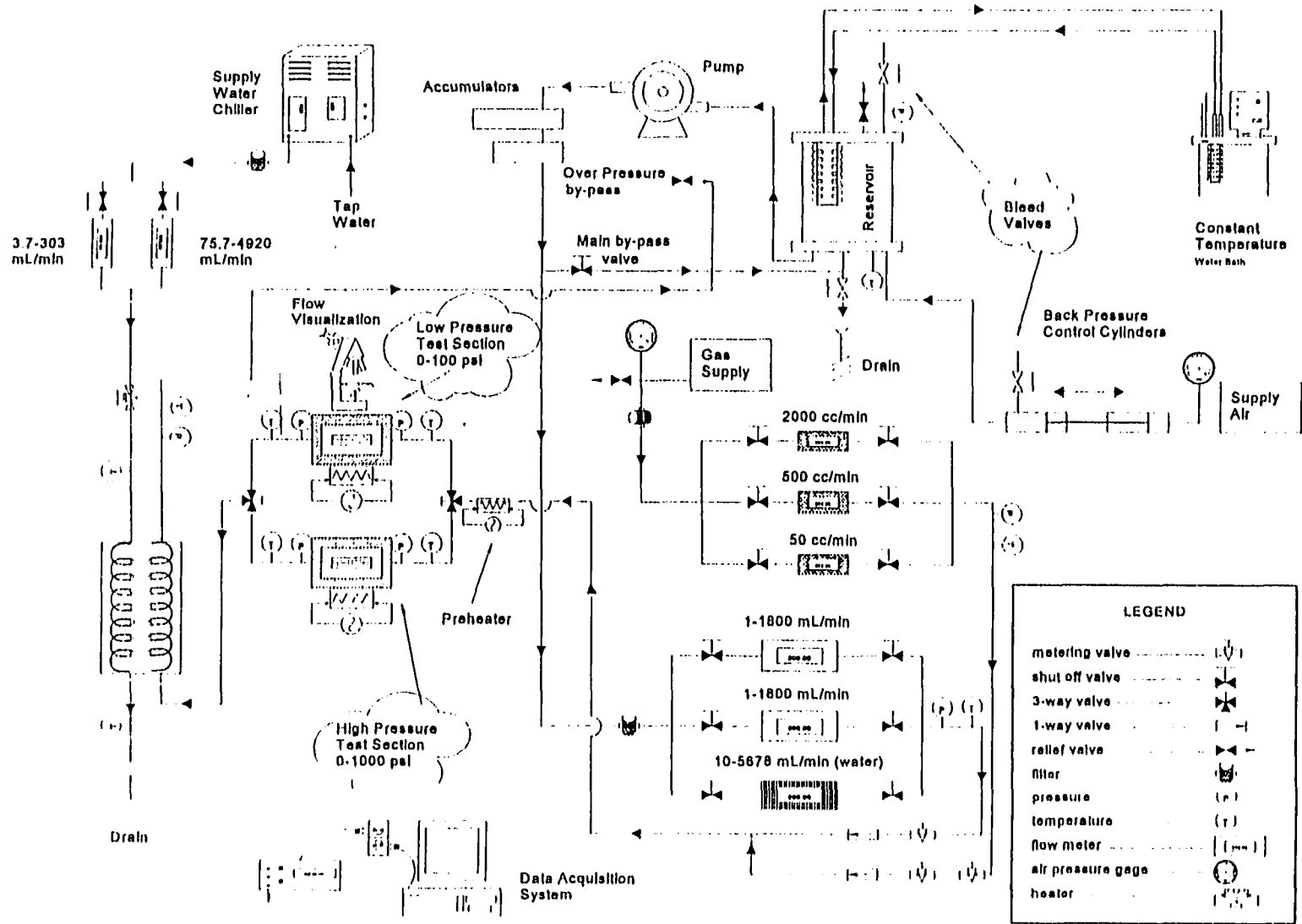


Figure 4.4: Schematic of experimental flow loop

psig) and pressure differentials up to approximately 2000 kPa (300 psig) was chosen. The maximum flow rate was about 3800 cc/min (one gpm) which could be varied easily by adjusting the controller speed. Although the pump produced very little pulsation, a pulse damper and two accumulators were added to the system to lessen the pulse effect.

The flow meters used for this research are shown in Figure 4.5. The water flow meter (Max Machinery, model #234) had a range from 10 cc/min to 5,000 cc/min. There were two other flow meters (Max Machinery, model #213) for non-aqueous liquids with a capacity from 1 to 1,800 cc/min each, and they were used for the present study. The precision of these will be discussed in the error-analysis section. There were also three gas flow meters manufactured by Omega with flow rates ranging up to 2,500 cc/min which may be used by other researchers in future.

The pressure transducers were chosen based on the maximum pressure expected from water pump (approximately 8,300 kPa /1,200 psig). Therefore, these were chosen with a rated capacity of about 6,900 kPa (1,000 psig) with proof pressure up to 10,400 kPa (1,500 psig). High-precision pressure transducers (OMEGA, PX-951) were used in the test section, while lower precision transducers (OMEGA, PX-213) were used elsewhere in the flow loop for economic reasons. These pressure transducers have a temperature limitation of approximately 85°C, which was the limiting component in the test fixture.

A secondary flow loop was used to cool down the temperature of the fluid past the test section. It also served as a condenser in case of flow boiling in the test section. It was basically a counter-flow double pipe heat exchanger. Chilled water was used as

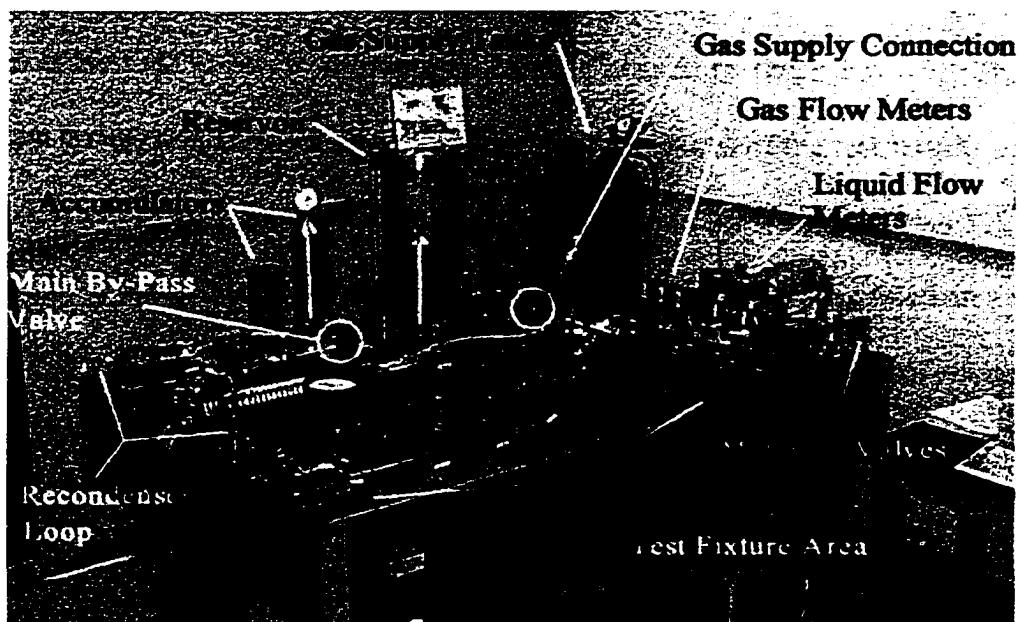


Figure 4.5: General layout of flow loop components

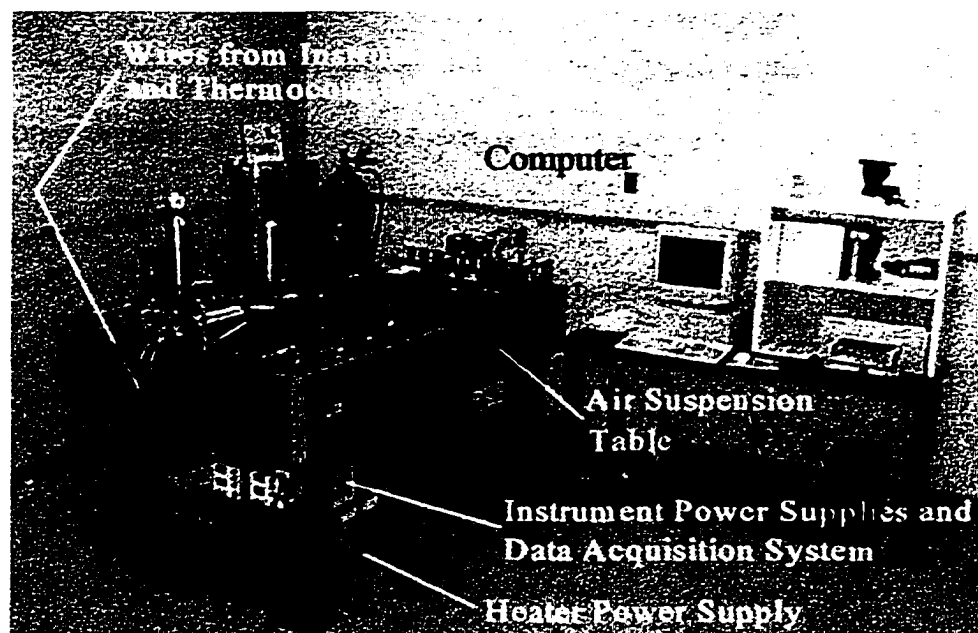


Figure 4.6: General layout of entire flow loop apparatus

the coolant because of its large specific heat. Therefore, it could remove more heat from the test fluid at a moderate flow rate. However, the amount of subcooling was limited to 10 °C in the present study.

The data acquisition system consisted of a Dell personal computer with HP 34970A for Windows data acquisition package. All temperatures, pressures, and flow rates were monitored in real time and displayed on the monitor allowing the user to determine when steady state has been reached. The data acquisition system was set up to measure all quantities 512 times per second, and the data output to the screen was updated approximately once per second. The raw data were stored in an Excel spreadsheet when desired.

An electric heater was used to heat up the fluid in the test section. The voltage (V) and current (i) were read directly from it, and the power supplied was calculated from the relation

$$\text{Power, } P = Vi \quad (4.20)$$

The test section and test fixture components are shown in Figures 4.7 and 4.8. The test fixture is represented in more detail in Figures 4.9 and 4.10 with the test section removed. The O-ring grooves, thermocouple wire slots, heater, heater power wires, etc., could be clearly seen from these figures.

### **Experimental Procedure**

A brief description of the experimental methodology followed in this study is provided in this section. To begin, all power supplies, the computer and the data acquisition were turned on. Approximately thirty minutes were allowed for the



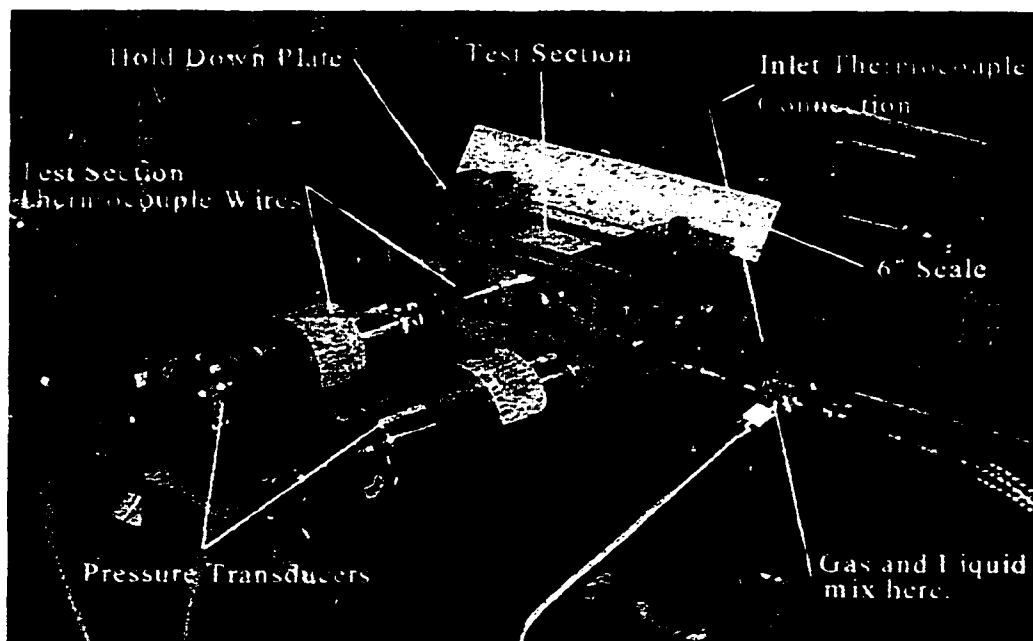


Figure 4.7: Test fixture components

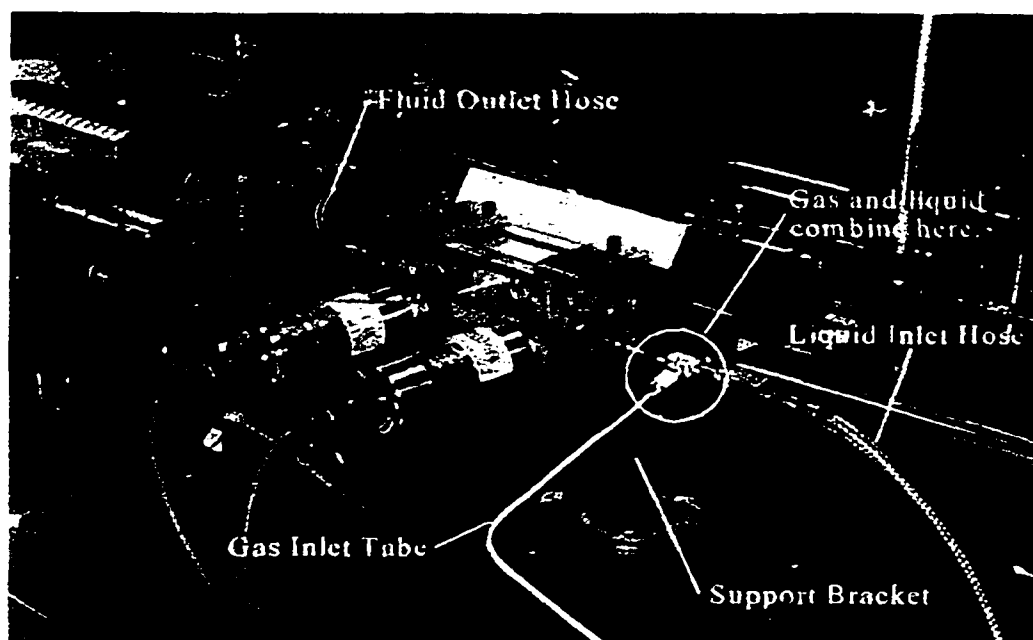


Figure 4.8: Complete view of test fixture

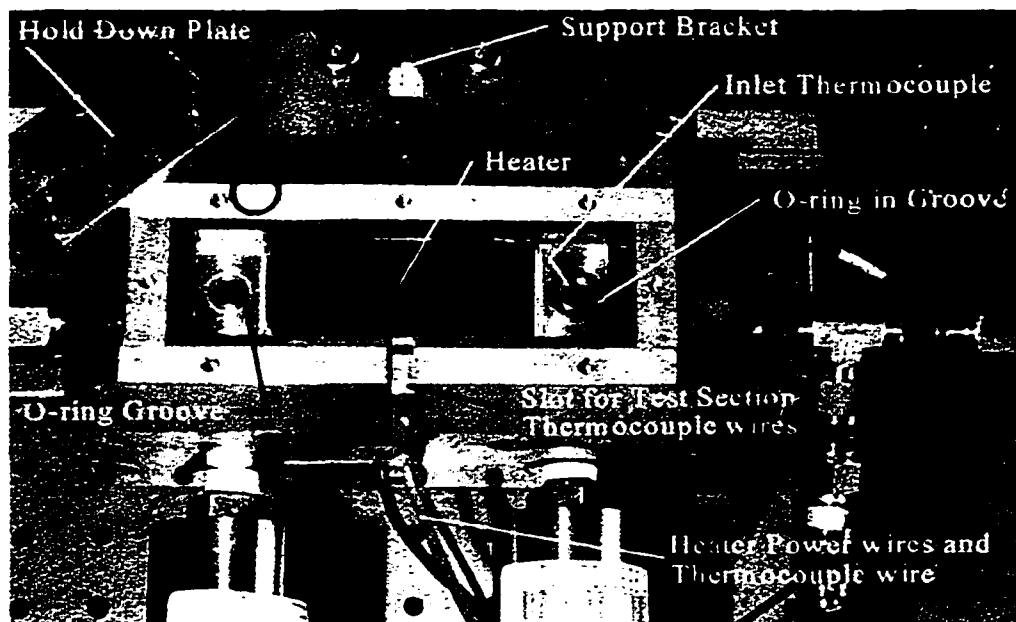


Figure 4.9: Detail of test fixture components without test section

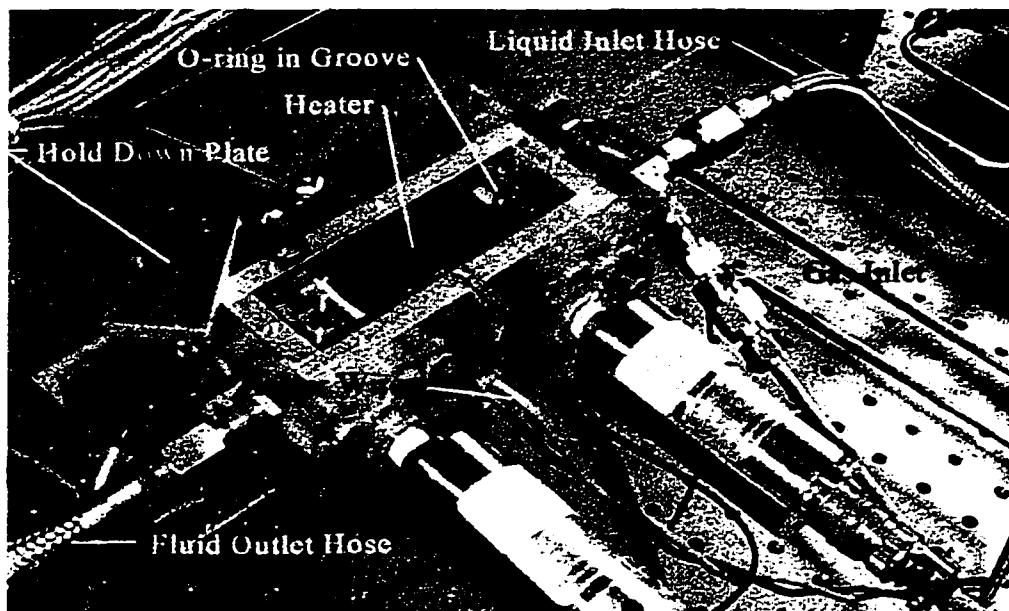


Figure 4.10: Detail of test fixture without test section installed

instruments to come to operating temperature. During this period the data acquisition program was started, and the temperatures and pressures were monitored to determine whether those instruments were functioning properly.

The heater was coated with a thin layer of Omegatherm high-thermal conductivity grease to ensure an even distribution of heat energy to the test section. Then new o-rings were placed in the o-ring grooves in the test fixture. For better sealing, it is always a good idea to replace the o-rings each time a test section is removed. Once this routine was performed, a test section was installed in the test fixture. The test section was pressed down firmly and bolted on hold down plates. The bolts were only finger tightened since use of any mechanical device could have resulted in over-compressing the o-rings and breaking the glass cover plates. Then the thermocouples were connected, and the thermocouple readings were checked to make sure they were functioning properly.

The liquid flow loop was then started by turning on the pump. Before the pump was turned on, the main by-pass valve (Figure 4.4) was kept open and the metering valve downstream of the liquid flow meter was kept closed. One also has to be careful with the flow meter valves so that liquid passes only through the designated flow meter, and not through one which is not supposed to handle the liquid. There was also an additional by-pass line around the test fixture. The multi-way valves were switched so that the liquid will flow through the by-pass only. At this point, the pump was turned on. After a few minutes, the metering valve downstream of the liquid flow meter was completely opened while gradually closing the main by-pass valve. As the valve was closed, the accumulators slowly began to fill and the flow rate and pressure

at the liquid flow meter gradually increased. The pressure downstream of the liquid flow meter was monitored with the main by-pass valve completely closed. Since the flow rate and pressure from the pump are below the limiting conditions of the flow meter, any unexpected rise in pressure is an indication that the microfilter is getting clogged and needs to be replaced. The system is run for a few minutes with the main by-pass valve closed and then it is slowly opened allowing the system to return to normal condition.

Now the multi-way valve is switched so that the fluid will flow through the test section. Because the liquid flow meter reading was found to be unsteady at low flow rates, it was measured only after setting the test section inlet pressure using the metering valve. Since a moderate lag time exists between adjustment of the valve and stabilization of test section inlet pressure, the liquid metering valve was adjusted very slowly. The inlet pressure could be controlled within  $\pm 0.5$  psi for this system.

Once a steady flow was established through the test section, the heater power supply was turned on and the output was adjusted to establish a temperature difference across the test section. The heater was powered by a 150V, 35A, DC power supply. A DC power supply is recommended because an AC power supply generates an induction voltage which may interfere with the readings of the thermocouples near the heater and heater wires. However, one should be careful about the fact that turning the heater on without any fluid flowing through the test section may damage the test section as well as the test fixture. The temperatures of the heater, test section wall, inlet, and outlet temperatures were monitored to prevent any damage while adjusting the power supply. The following maximum temperatures are recommended for safe

operation of the experimental apparatus: (1) heater temperature should not exceed 160°C, and (2) test-section wall, inlet, and outlet temperatures should not exceed 60°C. The system is then allowed to reach a steady state before any data could be recorded.

Depending on the heater voltage the system took about ten to fifteen minutes to have a steady-state temperature distribution. Once the temperatures had stabilized, the data were recorded through HP data-acquisition software. The data were recorded at an approximate rate of two measurements per second. For statistical purposes, which will be discussed in the error-analysis section, thirty data points were recorded for each setting. The fluid flow rate was then adjusted for the next data point.

Occasionally, the heater output had to be adjusted to establish a reasonable temperature difference as the flow rate was adjusted. Every time an adjustment was made, it was necessary to wait until a steady-state condition was reached. The amount of time required depended on the magnitude of changes in flow rate and/or heater output. Since the temperatures and pressures were monitored in real time, one could easily notice whether a steady-state condition has been reached or not. When all the data points have been recorded, the system was ready to shut down.

To shut down the system, first the heater was turned off with the fluid still flowing through the test section, thus allowing the test section and fixture to return to room temperature. Secondly, the liquid metering valve was closed and the main bypass valve was slowly opened reducing the pressure to the flow meter to its starting value. Only at this point, the pump could be turned off as well as the computer and data acquisition system.

### **Data Reduction Technique**

The raw data generated from the experiments were stored in Microsoft Excel file. The data were then used in determining the fluid properties, fluid flow and heat transfer parameters. The calculations used in converting the raw data and in determining the flow and heat transfer parameters are presented in this section. All temperatures were stored in units of degrees Celcius. However, pressure readings were stored in terms of voltage while the liquid flow meter readings were stored in hertz.

The outputs measured in terms of volts or hertz were converted to appropriate units. For example, the pressure transducers had an output range of 0.0 Vdc – 5 Vdc. So the voltage signal was converted to the corresponding pressure by the equation

$$\text{Pressure (gage)} = \frac{\text{voltage} - \text{offset}}{5.0} (\text{max. pressure range}) \quad (4.21)$$

where voltage is the value recorded by the data acquisition system, offset is the calibration voltage measured while the transducer was open to atmospheric pressure, and maximum pressure range is the capacity to which the transducer is calibrated (1000 psig for this study). The liquid flow meter conversion was performed using the K-factor provided by the manufacturer (Max Machinery). The equation is

$$K \times Q = f \quad (4.22)$$

where K was in pulse/cc, f was the measured output in hertz (pulse/second), and Q (cc/second) was the flow rate to be determined. The accuracy of the equation was listed to be +1%/-6% over the entire range of the flow meter (1 – 1800 cc/min).

Several fluid flow and heat transfer parameters were calculated to analyze the experimental results. The equations presented in this section were used to calculate the

parameters listed in Appendix B. Since all these parameters are average values, the fluid properties were determined from the average temperature and pressure measured between the inlet and outlet of the test section.

To determine the Darcy friction factor, the following parameters were calculated. Velocity was obtained from the continuity equation as

$$\bar{V} = \frac{\dot{V}}{A} \quad (4.23)$$

where  $\dot{V}$  is the measured volumetric flow rate, and A is the cross-sectional area of the channel (width x height). Another important parameter for fluid flow, the hydraulic diameter was calculated as

$$D_h = \frac{4A}{P} \quad (4.24)$$

where P is the wetted perimeter defined as 2 x (width + height) for rectangular channels. From these definitions, the Reynolds number is calculated from

$$Re = \frac{\rho \bar{V} D_h}{\mu} \quad (4.25)$$

where  $\rho$  and  $\mu$  are the average fluid density and absolute viscosity, respectively. The Darcy friction factor is given by

$$h_f = \frac{f L \bar{V}^2}{2 g D_h} \quad (4.26)$$

where  $h_f$  is the pipe head loss, L is the channel length, and g is the acceleration due to gravity. This head loss is also given by

$$h_f = \frac{\Delta p}{\rho g} \quad (4.27)$$

Combining the two equations for head loss and solving for friction factor yields

$$f = \frac{2\Delta p D_h}{\rho L \bar{V}^2} \quad (4.28)$$

where  $\Delta p$  is the pressure drop measured across the channels.

However, the expression does not consider the minor losses due to sudden contraction and expansion of the fluid as it enters into or exits from the microchannels. One way of determining this effect is by using the loss coefficients associated with contraction and expansion. By assuming that the flow has a uniform velocity while entering the tubes, Kays (1950) showed that the expansion and contraction loss coefficients are best represented by the following equations

$$K_E \approx 1 - 2\sigma K_d + \sigma^2 \quad (4.29)$$

$$K_C \approx \frac{1 - 2C_C + C_C^2(2K_d - 1)}{C_C} \quad (4.30)$$

where  $\sigma$  is the free flow to frontal area ratio,  $C_C$  is the contraction ratio and  $K_d$  is the velocity distribution coefficient. The method of calculating these parameters has been described in detail by Bailey (1996). Kays (1950) also presented these loss coefficients for different geometries using the above equations. Since these coefficients are dependent on Re numbers, their values may be estimated from Kays (1950) results, once Re numbers are known from the experimental results. After incorporating the loss coefficients, the expression for friction factor takes the following form

$$f = \frac{2\Delta p D_h}{\rho L \bar{V}^2} - (K_C + K_E) \frac{D_h}{L} \quad (4.31)$$



Considering the range of Re number in this study and for rectangular channels, a conservative estimate for the coefficients was found to be  $K_C = 0.51$  and  $K_E = 1.0$ . Considering the worst situations, when the first term of equation (4.31) was minimum due to high Re number (channel C2) and also when the second term of equation (4.31) was maximum due to largest hydraulic diameter (channel B), maximum deviation was found to be approximately 16.5%. Subsequently, equation (4.31) was used for calculating the friction factor.

For heat transfer analysis, the parameters of interest were heat transfer coefficient and Nusselt number, both determined according to the following procedure. As the fluid flows through the microchannels, the heat transferred to the fluid is given by

$$q = \dot{m}C_p(T_{\text{out}} - T_{\text{in}}) \quad (4.32)$$

Or, in terms of volumetric flow rate,

$$q = \dot{V}\rho C_p(T_{\text{out}} - T_{\text{in}}) \quad (4.33)$$

The heat transfer coefficient is determined by equating the amount of heat transferred to the fluid to the amount of heat transferred from the channel walls. From Newton's law of cooling, the heat transfer coefficient is defined as

$$q = A_w h(T_w - T_\infty) \quad (4.34)$$

where  $A_w$  is the wall area of the channel over which heat is transferred,  $T_w$  is the average channel wall temperature, and  $T_\infty$  is the bulk fluid temperature. The channel wall temperature was determined by averaging the readings of the thermocouples numbered 1, 2, 4, 6, and 7 of the test section wall. Since these thermocouples were

located down the center of the channels, they were expected to give a reasonable estimate of the wall temperature. Moreover, because the channels were covered with glass plate, the top wall was considered adiabatic. Therefore, the wall area over which heat was transferred to the fluid was given by

$$A_w = L(2 \times \text{height} + \text{width}) \quad (4.35)$$

Equation (4.31) can be solved for the heat transfer coefficient, which is

$$h = \frac{q}{A_w(T_w - T_\infty)} \quad (4.36)$$

From definition, Nusselt number can be calculated as

$$Nu = \frac{h D_h}{k} \quad (4.37)$$

where  $k$  is the thermal conductivity of the fluid, while other parameters have been defined previously. Another important parameter heat flux is defined as

$$q'' = \frac{q}{A_w} \quad (4.38)$$

### **Error Analysis**

This section outlines the procedure for determining the uncertainty of the derived result. Any type of experimental measurement requires an uncertainty analysis in order to be able to judge the quality of the data. Experimental results involve some level of uncertainty that may come from causes such as lack of accuracy in measurement equipment, random variation in the variables, and approximations in data reduction relations. All these individual uncertainties eventually translate into uncertainty in the final results. This factor is called propagation of uncertainty and is an important aspect of any engineering experiment. In this study, temperature,

pressure, and flow rates were measured and manipulated to calculate friction factor and Nusselt number, so an uncertainty analysis was performed for these two expressions with a 95% confidence level. These uncertainties can be divided into two broad categories, namely precision error and bias error.

### **Precision Error**

Precision error is the lack of repeatability due to random error in individual measurements, and its estimation depends on sample size. It is usually determined by repeated measurements of the variable of interest or repeated measurements in calibration tests. The measured data are used to compute the sample standard deviation of the measurements, called the precision index,  $S$ , in uncertainty analysis.

$$S_x = \left[ \frac{\sum_{i=1}^n (x_i - \bar{x})^2}{n-1} \right]^{1/2} \quad (4.39)$$

The precision limit,  $P_{x_i}$ , for a single measurement  $x_i$  can be estimated using the Student's  $t$  distribution:

$$P_{x_i} = tS_x \quad (4.40)$$

where  $t$  is a function of the confidence level (95% in this study) and the degrees of freedom (number of data values minus one). One should note that the value of  $t$  is independent of  $n$  for  $n \geq 30$  as it reaches an approximate value of two. Therefore it is desirable to obtain 30 or more data points for a single measurement during experimentation (which was done for this study). However, since it is desired to

predict the uncertainty in the mean,  $\bar{x}$ , of the measurements ( $x_i$ ), the results are converted as follows

$$S_{\bar{x}} = \frac{S_x}{\sqrt{n}} \quad (4.41)$$

and the uncertainty is given by

$$P_{\bar{x}} = tS_{\bar{x}} \quad (4.42)$$

But if the result,  $R$ , is a function of  $n$  measured variables,  $x_1, x_2, \dots, x_n$ , then the precision index  $S_R$  can be computed from

$$S_R = \left[ \sum_{i=1}^n \left( S_i \frac{\partial R}{\partial x_i} \right)^2 \right]^{1/2} \quad (4.43)$$

The partial derivatives,  $\partial R / \partial x_i$ 's, are called sensitivity coefficient and are evaluated at the average values of the  $x_i$ 's.

### **Bias Error**

Bias errors include those errors known but that have not been eliminated through calibration and other fixed errors that can be estimated but not eliminated from measurement process. It does not vary during repeated measurements of a variable and is independent of sample size. Accuracy of an instrument, and hysteresis effects are considered bias error. This is a systematic uncertainty and computed from

$$B_R = \left[ \sum_{i=1}^n \left( B_i \frac{\partial R}{\partial x_i} \right)^2 \right]^{1/2} \quad (4.44)$$

where the bias uncertainty  $B_i$ , is usually determined by using the manufacturer's specification, and the sensitivity coefficient has been defined before. With these two parameters calculated, the total uncertainty is given by

$$w_R = [B_R^2 + (tS_R)^2]^{1/2} \quad (4.45)$$

For this study, the friction factor is expressed in the form

$$f = \frac{2(P_{in} - P_{out})D_h}{\rho L \bar{V}^2} \quad (4.46)$$

Following the procedure outlined above, the precision index can be written as

$$S_f^2 = \left( S_{P_{in}} \frac{\partial f}{\partial P_{in}} \right)^2 + \left( S_{P_{out}} \frac{\partial f}{\partial P_{out}} \right)^2 + \left( S_{\rho} \frac{\partial f}{\partial \rho} \right)^2 + \left( S_{D_h} \frac{\partial f}{\partial D_h} \right)^2 + \left( S_L \frac{\partial f}{\partial L} \right)^2 + \left( S_{\bar{V}} \frac{\partial f}{\partial \bar{V}} \right)^2 \quad (4.47)$$

However, it should also be noted that since the average velocity ( $\bar{V}$ ) is calculated from flow rate measurements, it is necessary to perform an error estimate for the velocity term as well to determine the precision index and bias uncertainty. Bias error is computed using an equation of similar form by substituting the precision index by bias uncertainty of individual variables. Once the bias and precision error are determined, the uncertainty can be calculated from equation (4.44).

Similarly the expression for Nusselt number is

$$Nu = \frac{\rho \dot{V} c_p (T_{out} - T_{in}) D_h}{kL(2H + W)(T_w - T_{\infty})} \quad (4.48)$$

and using this equation (4.47) an uncertainty analysis was performed following the same procedure for friction factor. The following is a list of bias errors as specified by the manufacturers.

Table 4.3: Bias Error for Measured Experimental Variables

<b>Variable</b>	<b>Bias error</b>
Pressure	$\pm 0.15\%$ of full scale
Volumetric flow rate	0.75% of reading
Temperature	1.0 <sup>o</sup> C
Channel height (depth)	0.01%
Channel length	0.04%
Channel width	0.01%
Voltage	$\pm 0.1$ V
Current	$\pm 1$ mA

## **CHAPTER 5**

### **ANALYSIS OF RESULTS**

In this chapter, the experimental data are analyzed. The results are compared with the macroscale correlations presented in Chapter 3 and also with the results of other researchers presented in Chapter 2. Four channel configurations, namely B, C1, C2 and D (Table 4.1) were used in this study. Friction factor and Nusselt number are the two parameters analyzed in this study. Also, comparisons are made of other heat transfer quantities of interest such as heat flux and forced convection heat transfer coefficient. Due to limitations of the flow meter used in this research, most data were collected in the transition and turbulent flow regimes. Results are presented for individual channel configuration along with the uncertainty of measurement associated with individual measurements. Later, all results are combined in order to provide a comprehensive view of the findings of this study.

#### **Single-Phase Flow**

##### **Friction Factor**

Friction factor data for channel configuration B is presented in Figure 5.1. The Reynolds numbers ranged from around 2100 to 13000. The uncertainty of friction factor measurements varied approximately from 3% to 19% while that of Reynolds

number was within 10% for all measurements. The uncertainty is higher for friction factor measurements in low range of Reynolds number and decreases as the flow becomes completely turbulent. This pattern generated because the uncertainty associated with velocity measurements was the dominating factor in friction factor uncertainty analysis. Because the flow meter inaccuracy was high for lower flow rates (less than 30 ml/min.), it resulted in higher uncertainty in velocity calculations and hence the higher uncertainty in friction factor for lower flow rates. However, the uncertainty associated with Reynolds number measurements were roughly a fixed percentage of Reynolds number. As a result, the absolute values of Reynolds number uncertainty increased with higher Reynolds number. Figure 5.1 also compares the experimental data with macroscale predictions. These theoretically predicted values are calculated using Equation (3.13) proposed by Bhatti and Shah (1987). Results were within 19% to 23% of the theoretical prediction and were consistently lower than predicted. However, the trend of the experimental data matched with theoretical predictions for all channel configurations. Figure 5.2 presents the friction factor data for channel C1. The Reynolds number varied from 1200 to 6000. The error bars followed the same trend as in channel B with the friction factor uncertainty ranging from 4% to 13%. The results were within 9% to 18% of the predicted values using Equation 3.13. The friction factor data for channel C2 are presented in Figure 5.3. The Reynolds number ranged from around 1900 to 13000. Friction factor uncertainty was calculated to be varying from 3% to 22%. A comparison of the experimental data with theoretical prediction indicates that experimental results varied from 21% to 28% as compared with the theoretical predictions. Maximum deviation was observed in the



first data point where friction factor was predicted assuming laminar flow at a Reynolds number of 1957. However, a revised friction factor assuming transient regime indicated a deviation of about 20.5%. To elaborate this fact both curves (laminar and transition) are presented in that region. Figure 5.4 represents the experimental friction factor data for channel configuration D. Most of the data points were in transition regime with Reynolds numbers varying from 1300 to 4400. Friction factor uncertainty was calculated to be varying from 7% to 23%. A comparison of experimental data with theoretical values indicates that the results were within 10% to 18% of the predicted values. Observing the fact that the experimental data have the same trend as that of theory, it is also possible that the experimental curve is shifted from theoretical one due to a fixed bias error of the instruments at present unknown to the author. All the experimental data were plotted in one graph in Figure 5.5 and then compared with the results presented by Choi *et al.*(1991) using equation (2.8b) and also with that of Yu *et al.* (1994) using Equation (2.10b). However, those correlations as proposed by the two authors are valid for Reynolds numbers greater than 4000 and 6000 respectively. Figure 5.6 gives a curvefit for all the experimental data in turbulent ( $Re > 4000$ ) regime. Based on the data, the following correlation was proposed to fit the experimental data.

$$f = 0.24/Re^{0.25} \quad \text{for } Re > 4000 \quad (5.1)$$

### **Nusselt number**

Heat transfer results are expressed and correlated in terms of Nusselt number. The experimental results are compared with theoretical values as predicted by

Gnielinski correlation (Equation 3.18) for transition and turbulent flow regimes. Later the experimental data are compared with the correlation proposed by Peng *et al.* (1994a,b) for forced convective heat transfer given by Equation (2.3b).

Figure 5.7 represents the experimental Nusselt number for channel B. The results had an uncertainty ranging from 20% to 53%. As before, the uncertainty was higher for lower Reynolds number, i.e., lower flow rates. However, this time the uncertainties associated with temperature measurements were the dominating factor. The order of magnitude of temperature measurement uncertainty was 3-4 times higher compared to other contributing elements. Also, all Nusselt number calculations involved temperature differences. As a result, at lower flow rates, the uncertainties were higher when the temperature differences were small while the opposite was true for higher flow rates, thus giving lower uncertainty numbers. A maximum heat flux of  $16 \text{ W/cm}^2$  was achieved in this configuration. A comparison of the experimental data with theoretical prediction shows that results varied from 6% to 77% and were consistently lower than theoretical values. The deviation increased with Reynolds number. As a result, the experimental results tend to flatten at higher Re number although theory predicts a steady increase of Nu number indicating direct dependence on Reynolds and Prandtl numbers. Nusselt numbers for channel C1 are presented in Figure 5.8 with Nu number uncertainties ranging from 29% to 65%. A maximum heat flux of  $4.9 \text{ W/cm}^2$  was achieved in this configuration. Experimental results were found to be lower than predicted values ranging from 75% to 84%. Figure 5.9 represents experimental data for channel C2 with uncertainties ranging from 20% to 45%. A maximum heat flux of  $15.4 \text{ W/cm}^2$  was achieved in this configuration. The data were

lower than predicted values varying from 45% to 70% with the exception of the first data point. It was about 40% higher than laminar Nu number for constant heat flux. However, assuming transition regime at Re number 1957, experimental data point was 3% lower than predicted value as can be seen from the Gnielinski correlation. This comparison is more consistent considering the fact that experimental values have always been lower than theoretical predictions. However, there are insufficient data to suggest that transition was indeed achieved at that Reynolds number. Figure 5.10 gives the Nusselt number data for channel D with uncertainties ranging from 28% to 67%. A maximum heat flux of  $5.7 \text{ W/cm}^2$  was achieved in this configuration. Figure 5.10 also gives a comparison of the same data with theoretical values, which were consistently higher by 51% to 84%. Theory suggests that heat transfer is greatly enhanced in turbulent flow as a result of turbulent mixing among fluid particles. One possible reason for the large deviation of experimental data with predicted values is that the amount of turbulent mixing is limited by the size of the microchannels. Once that limit is reached, further enhancement of heat transfer is restricted by the physical size of the microchannels. Figure 5.11 provides a comparison of the experimental data of the present study with that of the research findings of Peng *et al.* (1994a, b) using Equation (2.3b). Although their experimental data were limited to  $Re \leq 3000$ , those results have been extended to match the Reynolds number of this study. Peng *et al.* (1994a, b) also used different coefficients based on geometric parameters (hydraulic diameter and aspect ratio) of the channels. Of those, only two different coefficients were used based on hydraulic diameters of the channels used in this study. Since it has not been established how aspect ratio of a channel affects the heat transfer rate, no

consideration was given to aspect ratio of the microchannels while choosing the coefficients. All these compromises had to be made due to non-availability of data that resembles the experimental conditions of this study. From the experimental data in Figure 5.11, it is apparent that two different factors that affect heat transfer took place in the microchannel configurations considered in this study. Heat transfer was much higher for channel configurations B and C2 compared with the other two sets of microchannels. These two channels (i.e., B and C2) had a larger hydraulic diameter than C1 and D, and they also had a high surface roughness. One possible explanation for this higher heat transfer could be attributed to the high surface roughness of those channels. As mentioned before, heat transfer rate is greatly enhanced in turbulent flow due to a phenomenon called turbulent mixing. For a given channel, this mixing can be improved by increasing the roughness of the channel walls, forcing the flow to become turbulent at a lower Reynolds number.

The primary objective to undertake in this research was to determine the feasibility of using liquid to cool electronic chips compared with cooling by air. While forced convection air cooling can provide up to  $1 \text{ W/cm}^2$  of heat removal, a maximum heat removal of  $16 \text{ W/cm}^2$  was achieved in the present study during single-phase experiments. Although this may be considered a significant improvement, the high pressure drops associated with high fluxes (about  $653 \text{ kPa}$  at  $16 \text{ W/cm}^2$ ) could be a limitation for electronic cooling. This would require the materials used for manufacturing of electronic chips to be strong enough to be able to handle such high pressures thus limiting the feasibility of electronic cooling using liquids. From similar research findings, Bowers and Mudawar (1994a, b) concluded that microchannels

should not be used unless high heat fluxes are required where weight and liquid inventory has to be minimum. However, it is worthwhile to investigate if this large pressure drop can be avoided by increasing the number of channels shorter in length, which was beyond the scope of this study.

### **Two-Phase Flow**

An effort was made to collect some data for two-phase flow. Channel B and C2 were used for this purpose. The heater power output was adjusted to ensure that the temperature at the outlet of the test section was above the boiling point of the refrigerant corresponding to the pressure at the inlet of the test section. As the channel wall temperatures were always higher than the outlet temperature, experimentation was limited to only low flow rates (less than 35 cc/min). This precaution was done not to exceed the upper limit of the test section temperature for safe operation, which was 60°C. Because the experimental apparatus did not have any provision to control the quality of the boiling fluid inside the microchannels, it always resulted in superheated vapor. This conclusion was drawn from the fact that the temperature distribution inside the microchannels never reached a steady-state condition. As the temperature steadily increased, a point was reached when the cover glass would shatter into pieces. This can be attributed to the fact that the rise in temperature in the test section caused thermal expansion of both the channel blank (aluminum) and the cover plate (Glass) which have different coefficient of thermal expansion. This difference in thermal expansion developed thermal stresses at the contact surface, which resulted in the shattering of the cover plate. Once a particular flow rate was established, the

temperatures at the inlet and outlet were determined mainly by the output from the heater. As a result, it was impossible to ensure that a chosen output from heater will result in a two-phase flow inside the microchannels. Also in absence of any optical device which would allow one to observe the formation of bubbles inside the microchannels, the heater output was always too high, producing superheated vapor. No data were collected after several failed attempts.

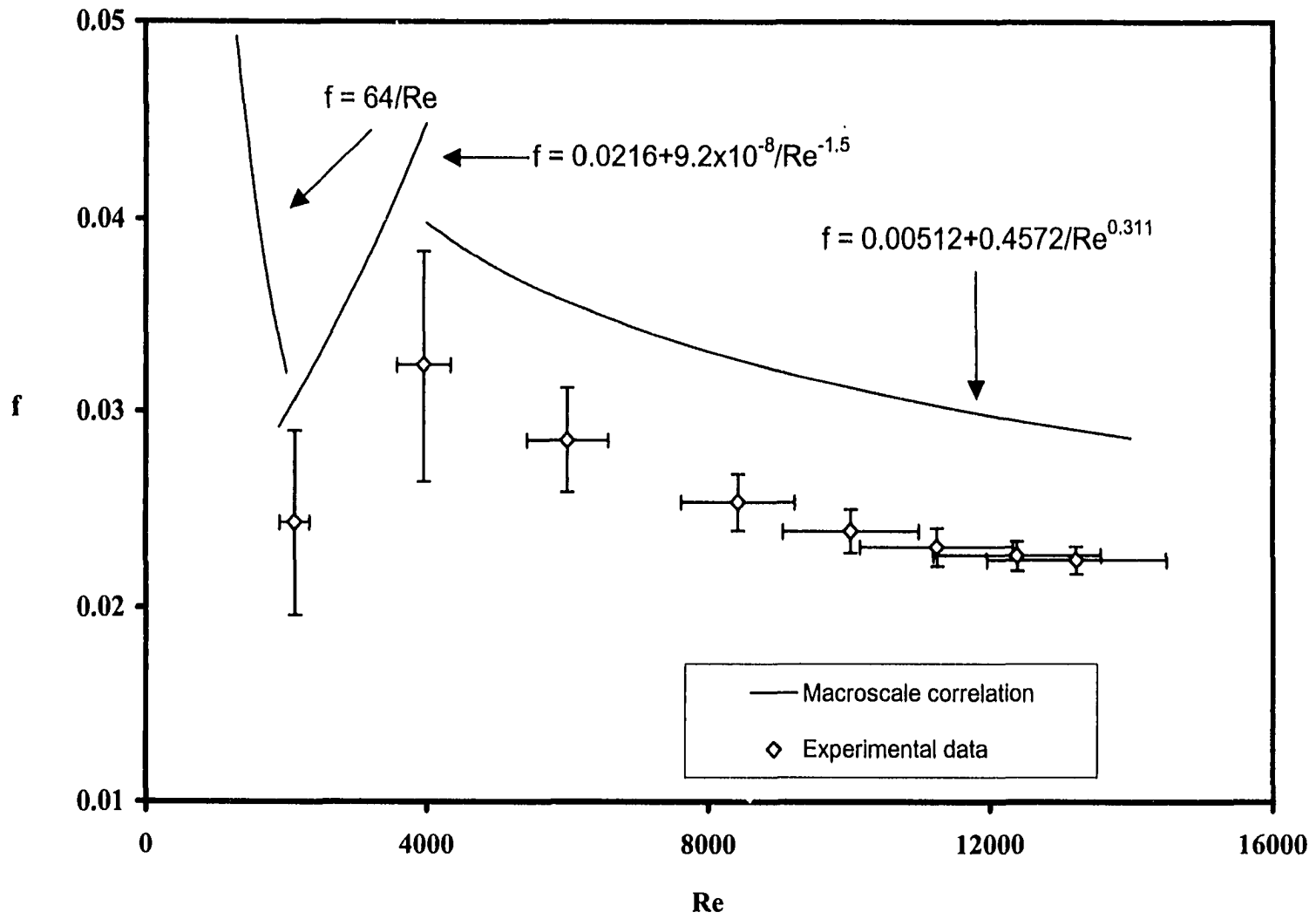


Figure 5.1: Friction factor for channel configuration B

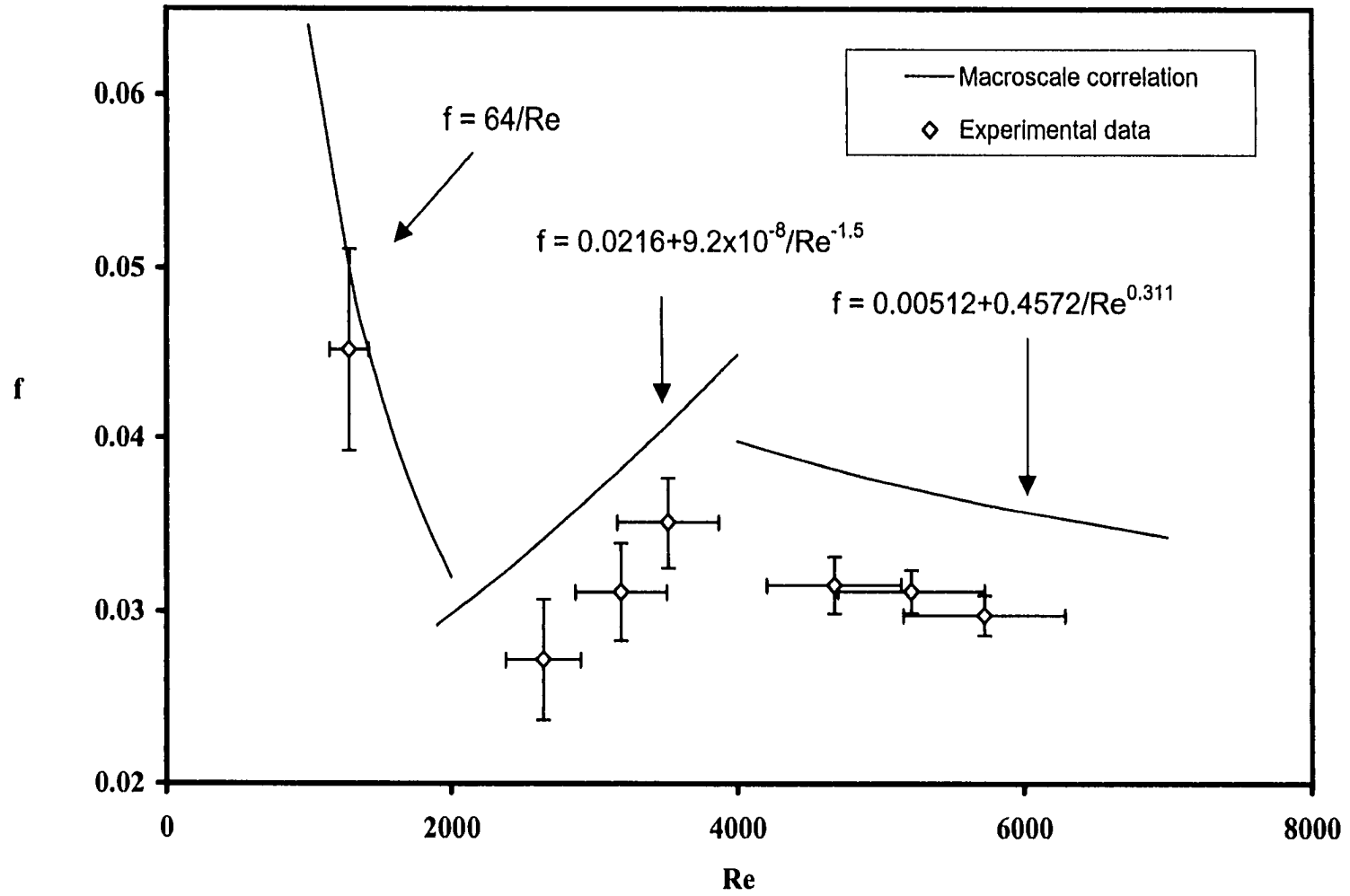


Figure 5.2: Friction factor for channel configuration C1



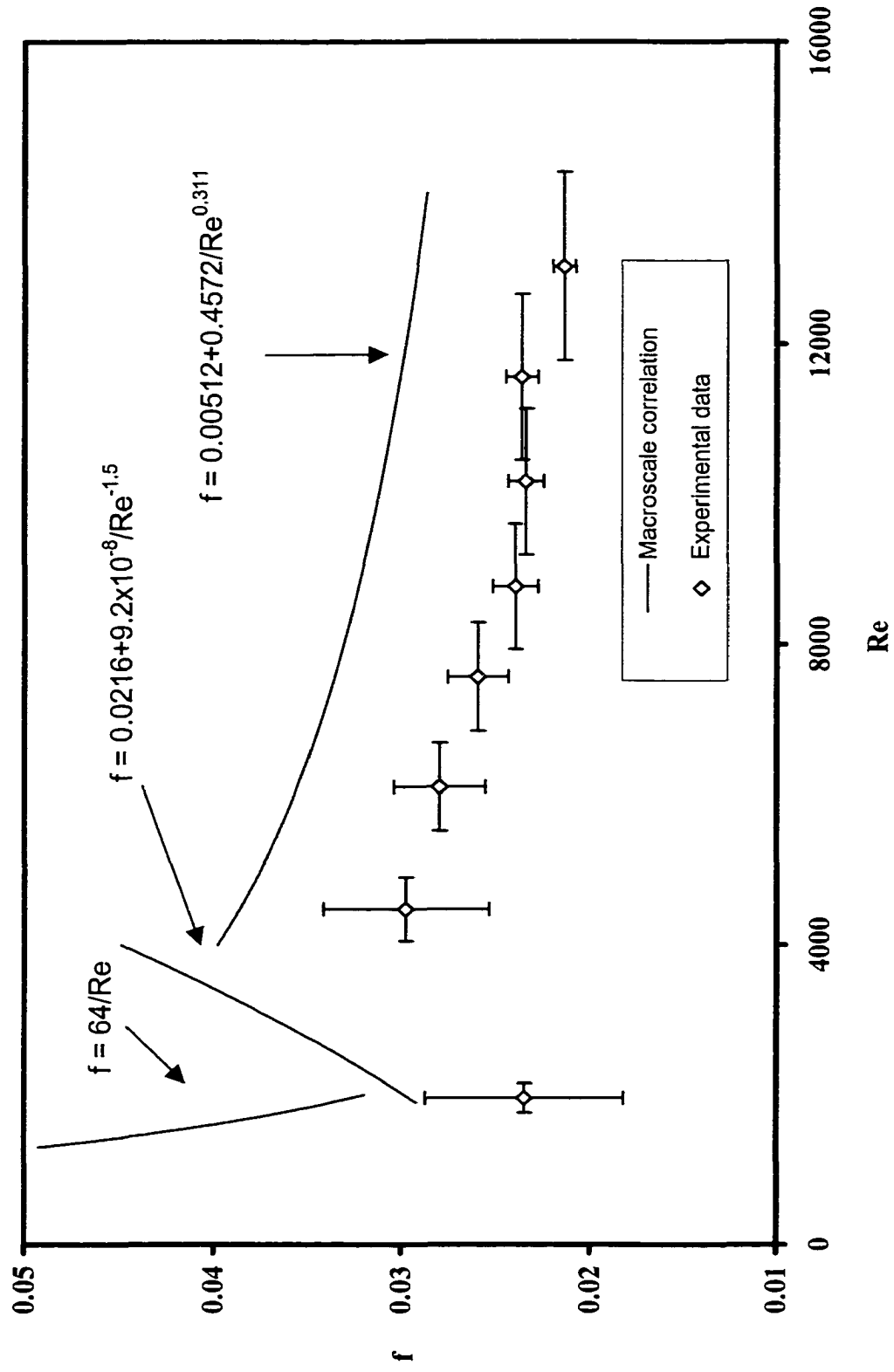


Figure 5.3: Friction factor for channel configuration C2

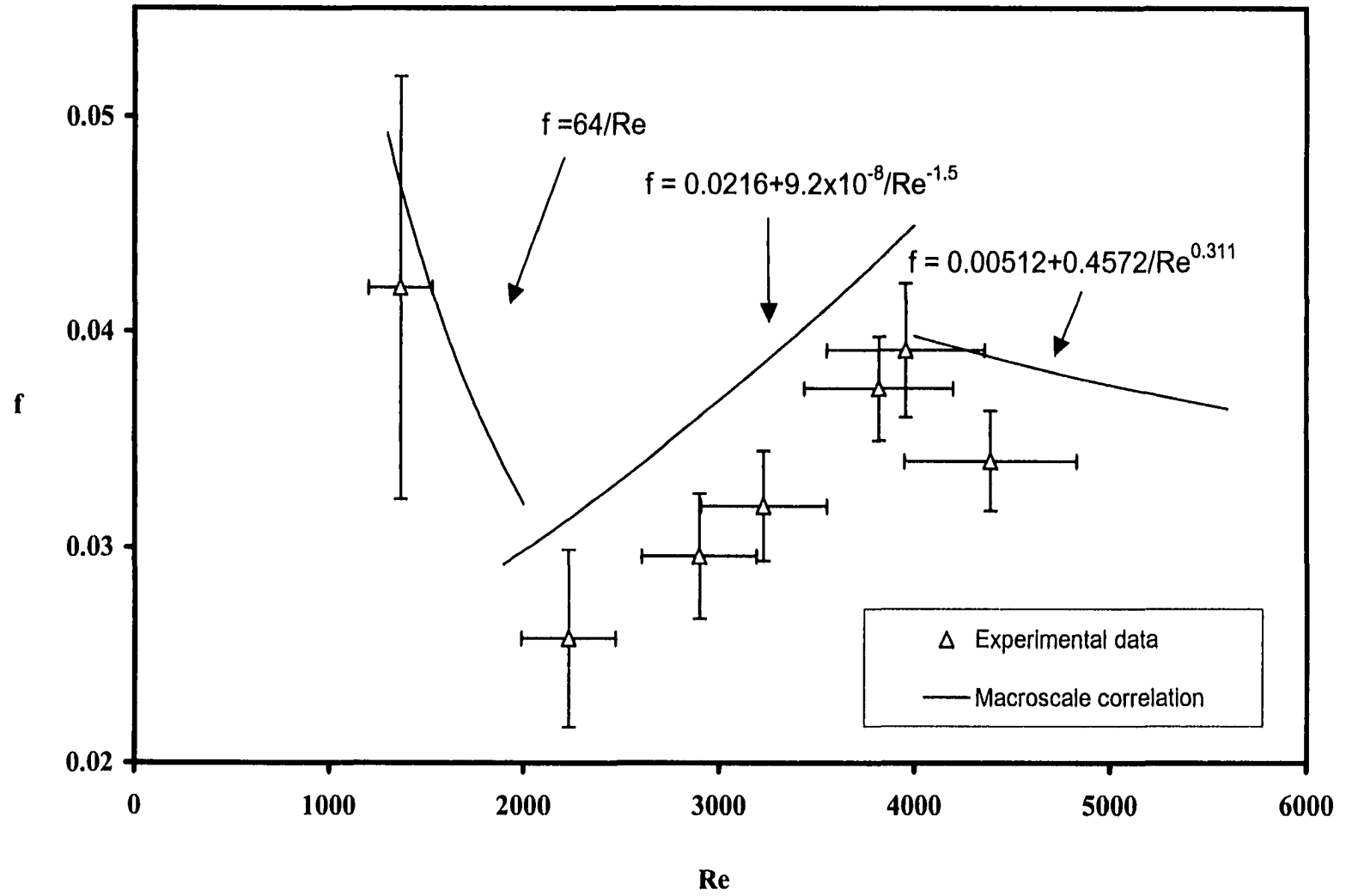


Figure 5.4: Friction factor for channel configuration D

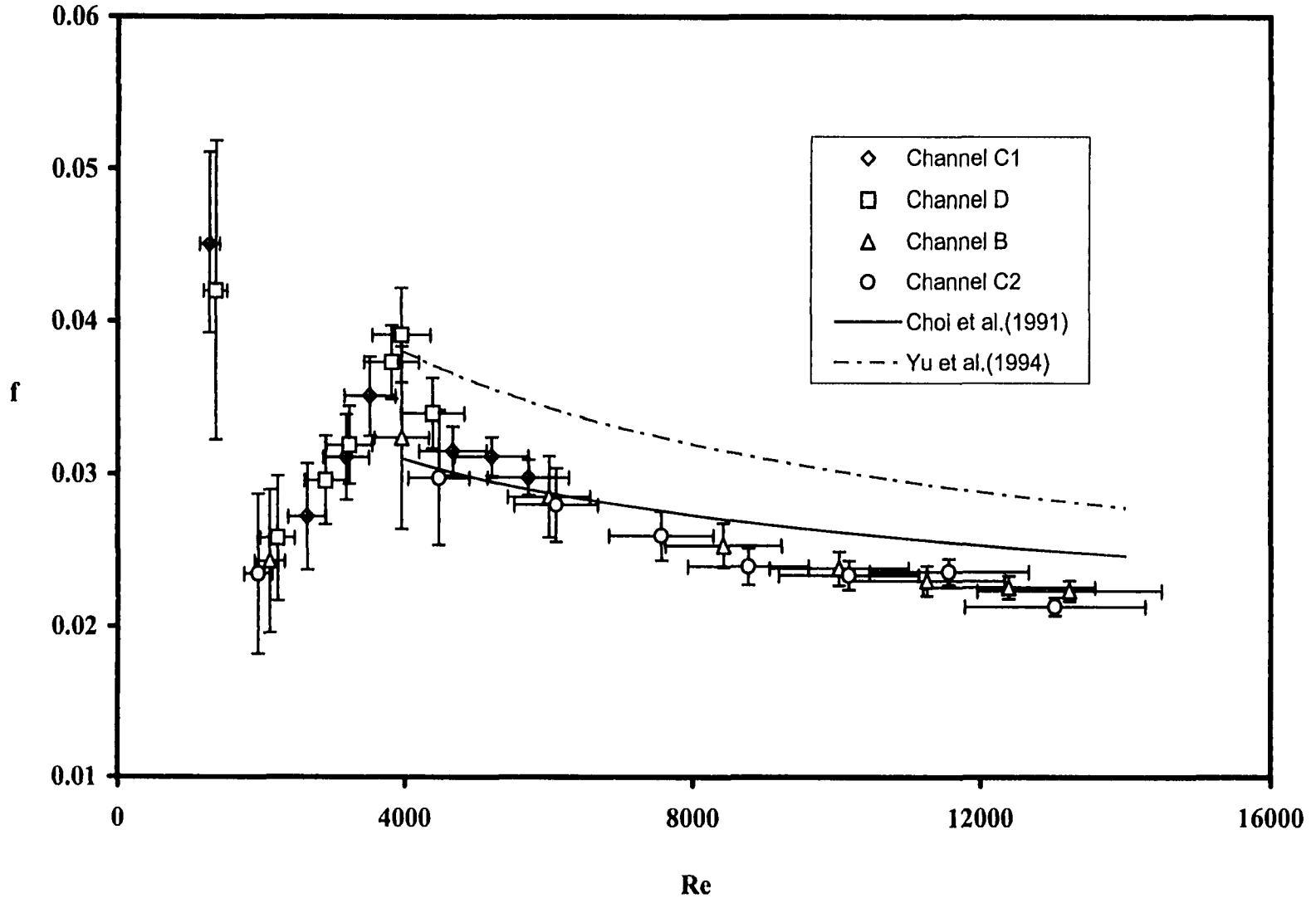


Figure 5.5: Friction factor comparison with Choi (1991) and Yu (1994)'s data

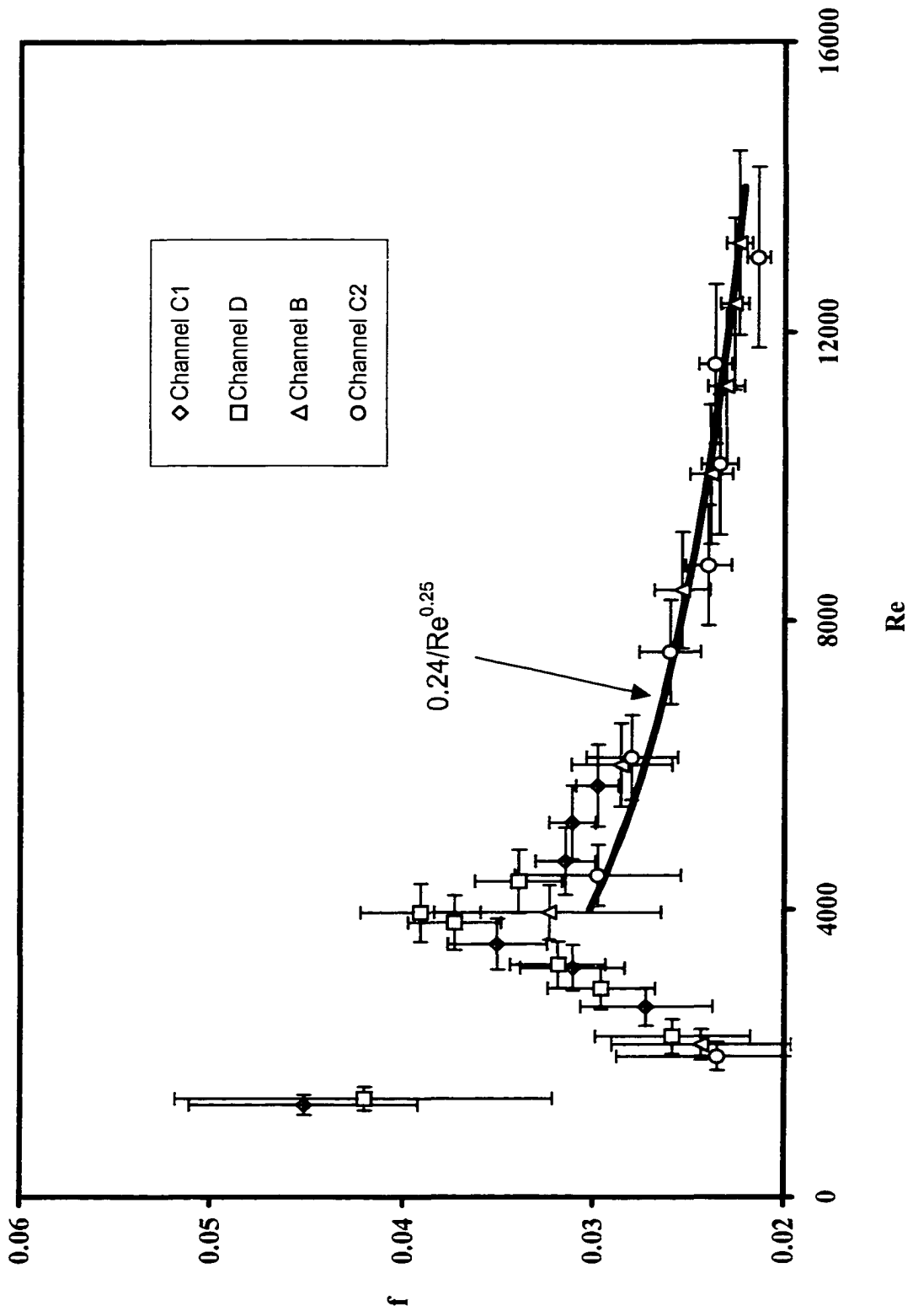


Figure 5.6: Curvefit of the experimental data

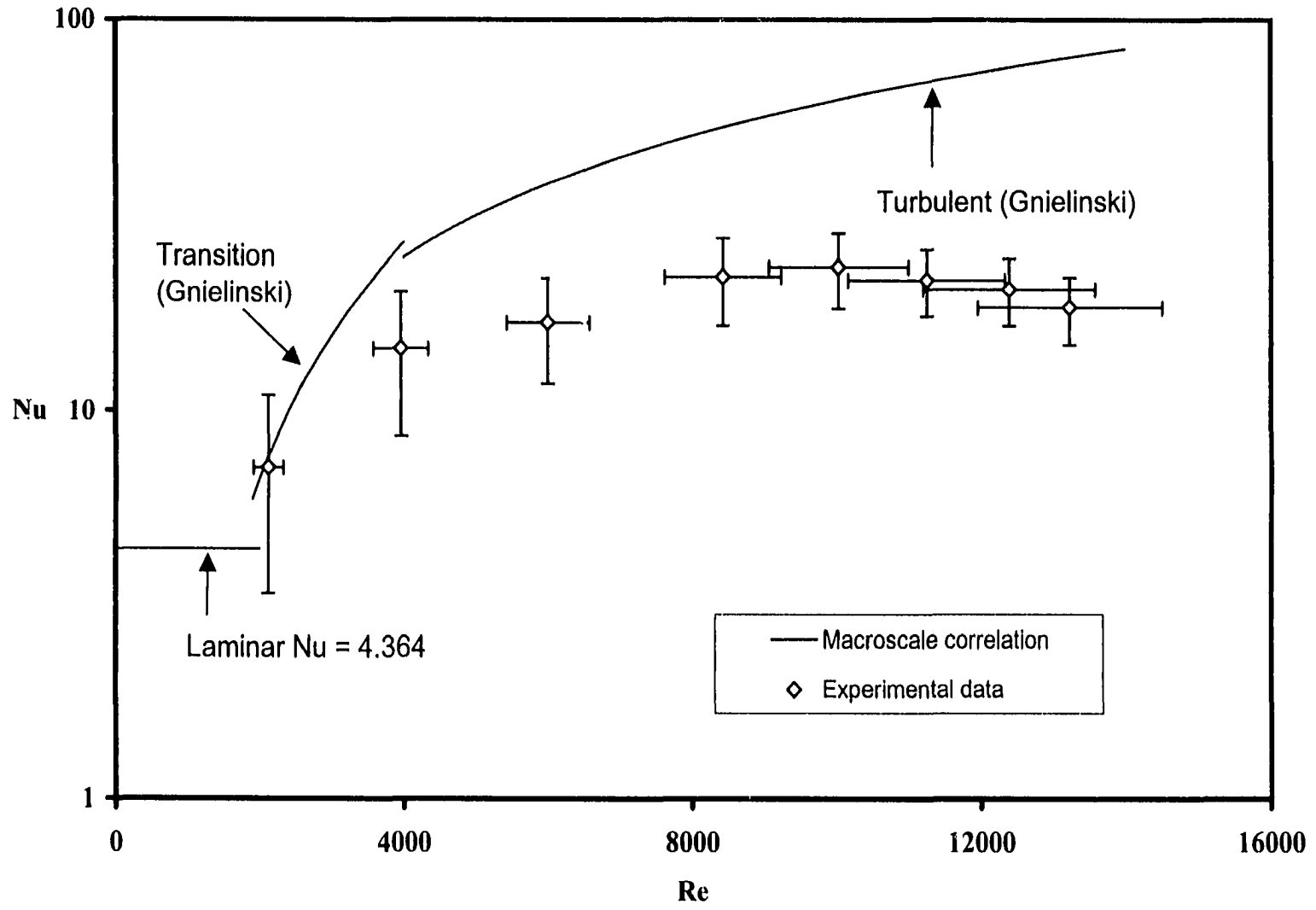


Figure 5.7: Nusselt number for channel configuration B

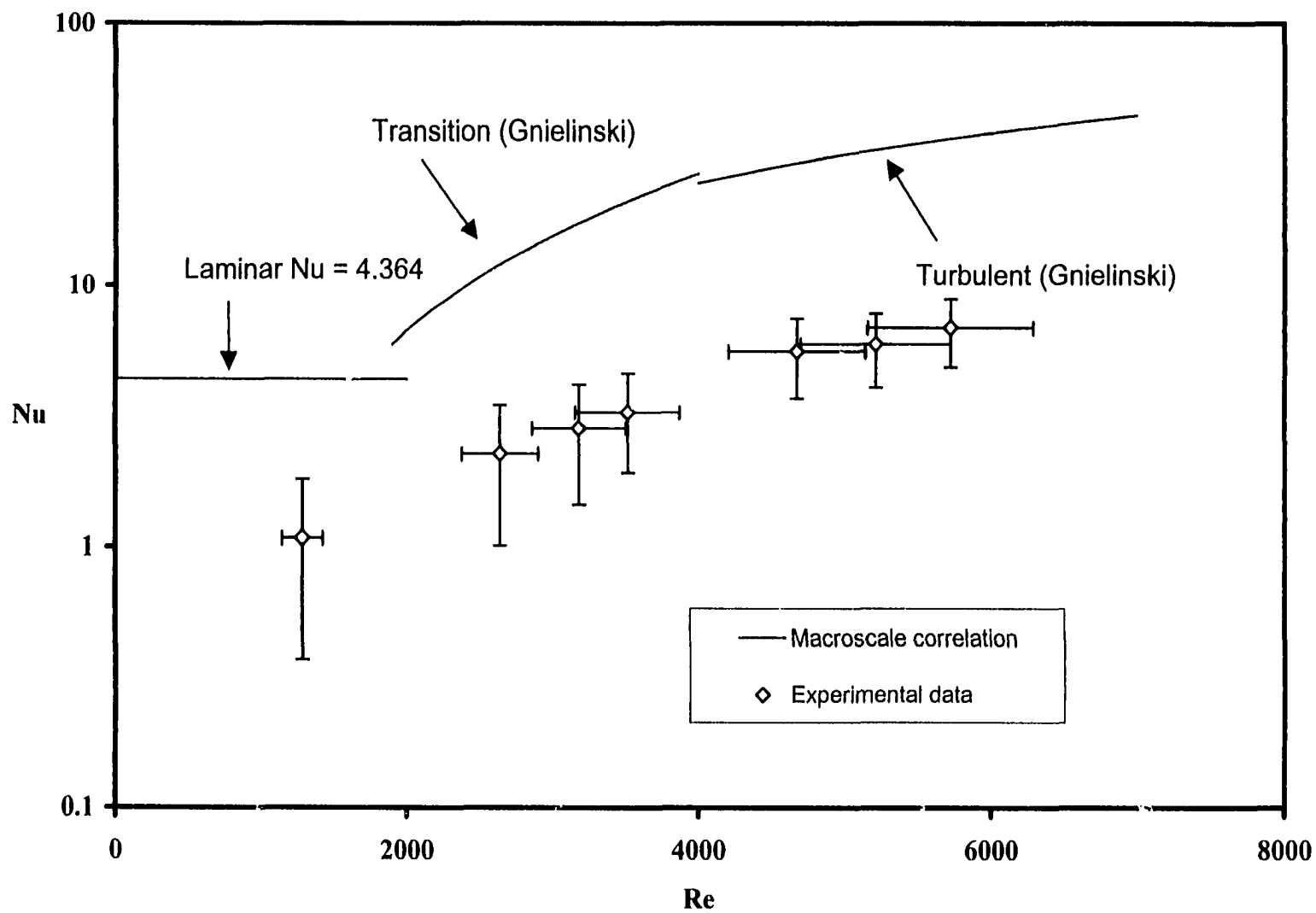


Figure 5.8: Nusselt number for channel configuration C1

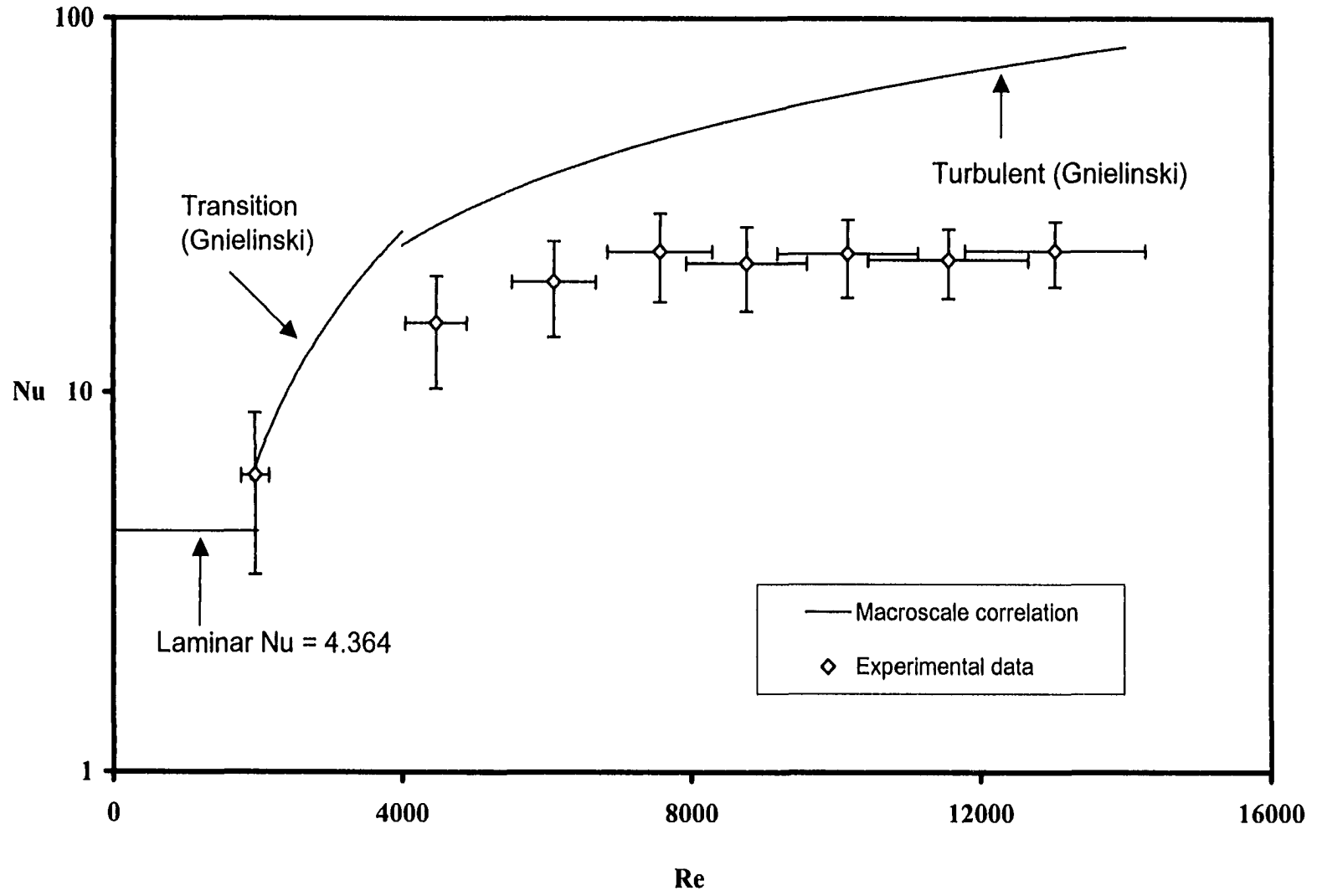


Figure 5.9: Nusselt number for channel configuration C2

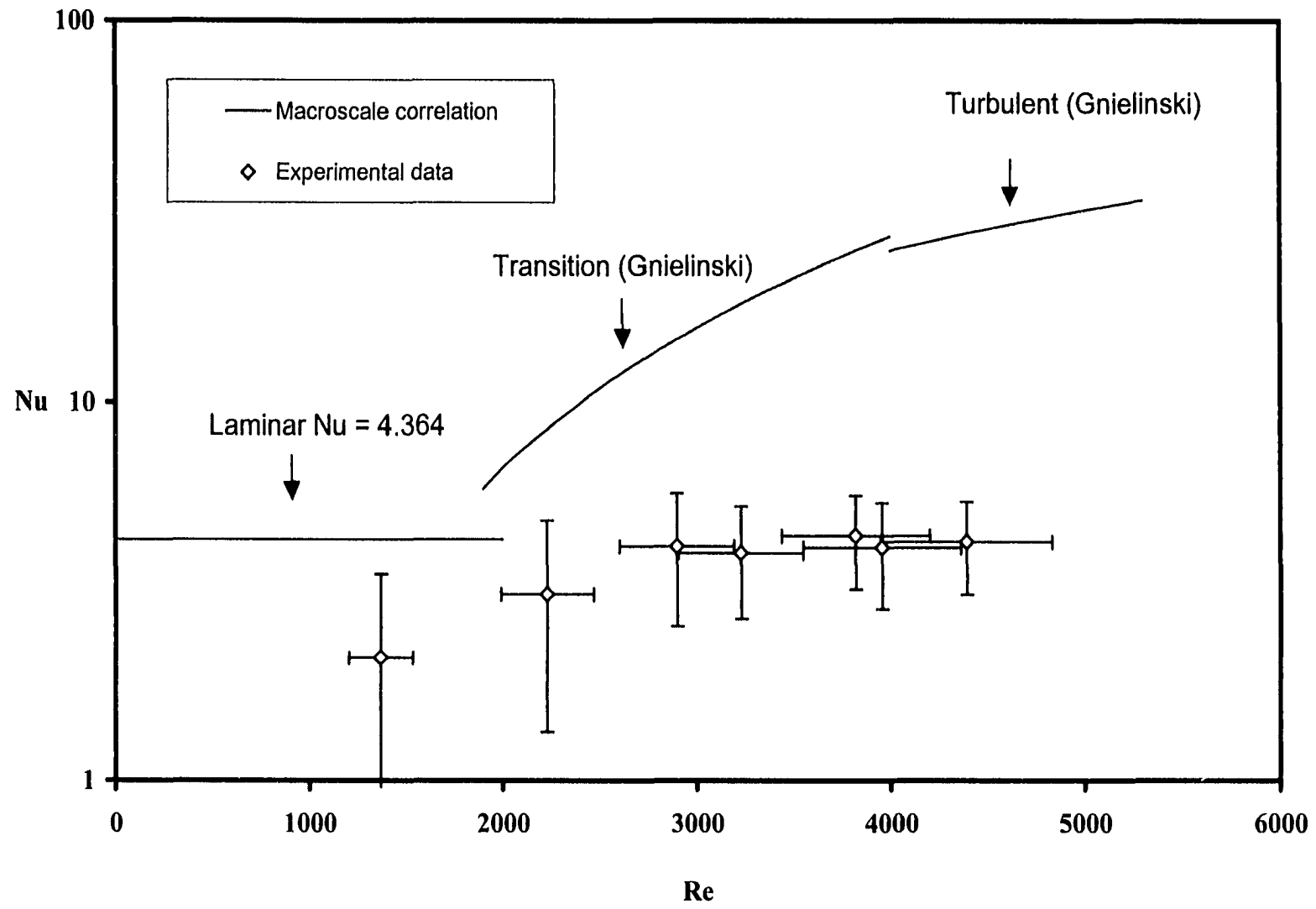


Figure 5.10: Nusselt number for channel configuration D



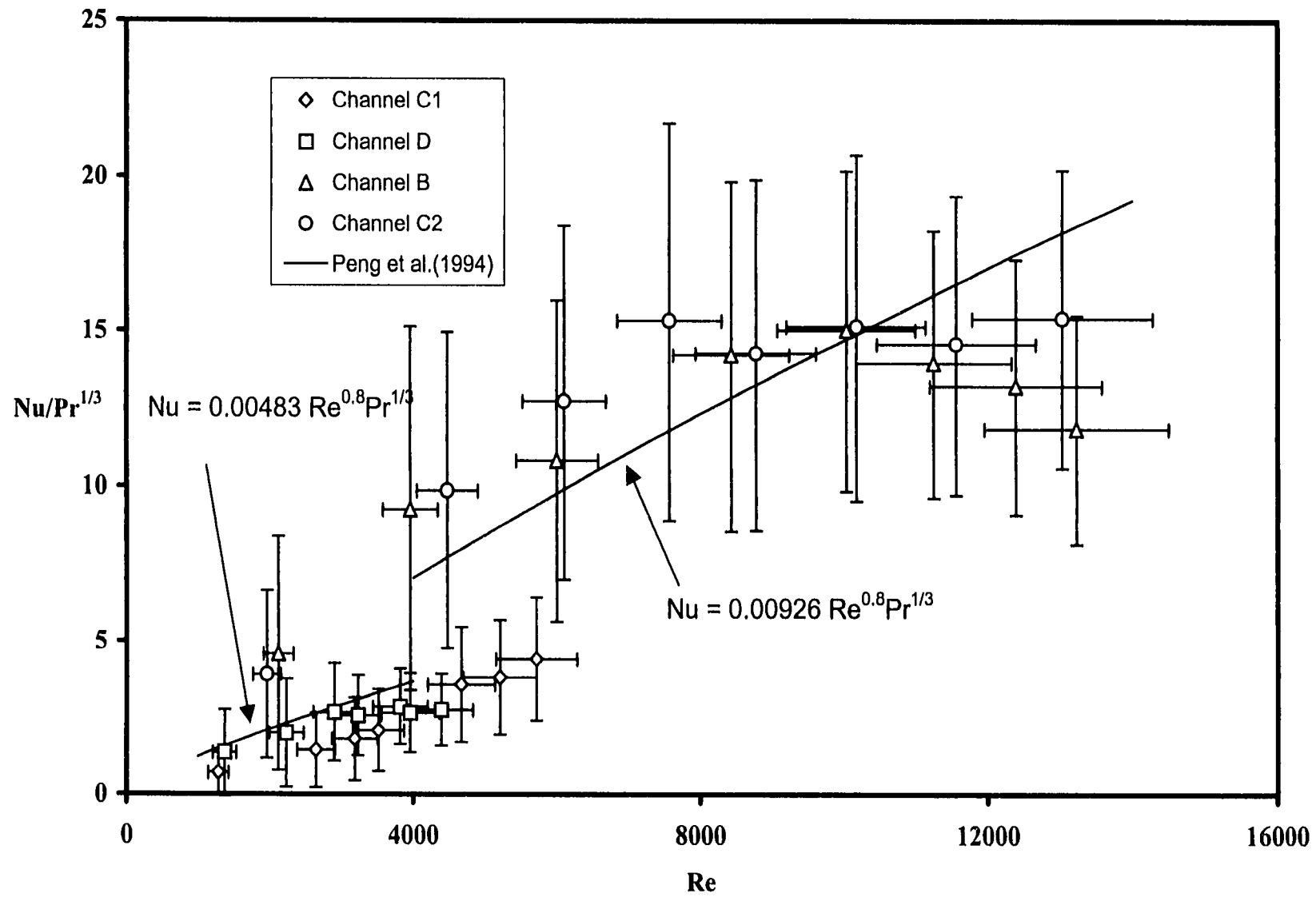


Figure 5.11 Nusselt number comparison with Peng et al. (1994)'s data

## CHAPTER 6

### CONCLUSIONS AND RECOMMENDATIONS

#### Summary of Present Study

This study concentrated on an empirical investigation of flow and heat transfer characteristics of refrigerant R-134A in microchannels. Four rectangular channel configurations were used to collect the experimental data, which ranged from 112  $\mu\text{m}$  to 210  $\mu\text{m}$  in hydraulic diameter. Three channels had an aspect ratio of approximately one while one had an aspect ratio of about 1.5. Microchannels were covered with glass to allow flow visualization during the experiments. However, no equipment was available for this purpose. A HP data acquisition system was used to monitor and store the necessary flow information during the experiments. Due to the limitations of the flow meter used in this research, most of the data were collected in the transition and turbulent flow regimes. Friction factor and Nusselt number were the two dimensionless parameters analyzed in this study. Comparisons were also made of other heat transfer quantities such as heat flux and forced convection heat transfer coefficient for different channel configurations. Correlations of the experimental data were presented and compared with other correlations provided by macroscale theory as well as by other researchers.

In determining the friction factor, one finds that velocity of the flow was the most critical parameter in this study. However, determination of velocity depended on

the accuracy of the flow rate measurement. Since the flow meter inaccuracy was high for lower flow rates (less than 30 ml/min.), it resulted in more inaccuracy in velocity calculations when the flow rate was low. This inaccuracy can be seen from the error bars associated with friction factor measurements. In order to avoid this, most of the measurements were performed for higher flow rates. As a result, very few data points were obtained for the laminar flow regime. The experimental results varied from 9% to 28% from the theoretical prediction and were consistently lower than the predicted values. The uncertainties associated with friction factor measurements ranged from 3% to 23%. Higher values of uncertainty were always associated with lower flow rates. However, the trend of the experimental curves matched with the macroscale predictions only shifted to lower values. This phenomenon could be produced due to a fixed bias error of the instruments at present unknown to the author. The experimental data matched reasonably well with the correlations proposed by two researchers (Choi *et al.* and Yu *et al.*) for completely turbulent flow in microtubes. The laminar results were found to be approximately 13% higher than reported by Yu *et al.* (1994). Due to lack of sufficient data and considering higher level of uncertainty in the laminar regime, no such comparison was made.

Nusselt number data did not yield any conclusive correlation in the present study. The experimental data deviated from the theoretical predictions ranging from 6% to 84%, deviation being higher for the smaller channels and also for higher Reynolds number for any given microchannel configuration. Although, theoretically, Nusselt number should increase steadily in macrochannels indicating its direct relationship with Reynolds and Prandtl numbers, this fact could not be established in

the present study with microchannels. One possible explanation for this deviation could be that the amount of turbulent mixing is limited by the physical size of the microchannels. This possibility could be ascertained by determining the Prandtl mixing length for turbulent flow and comparing it with the actual dimensions of the channels. However, this procedure requires knowledge of the local velocity profile inside the microchannels. Assuming a fully developed flow obeying “law of the wall,” Prandtl’s mixing length hypothesis for turbulence modeling (White, 1991) resulted in an approximate mixing length of  $54\ \mu\text{m}$  for smaller channels and about  $60\ \mu\text{m}$  for larger configurations (B and C2). Considering the fact that the smaller channels (C1 and D) have hydraulic diameters in the range of only  $110\ \mu\text{m}$ , size may have had an effect on heat transfer in those smaller channels. Also, in any turbulent flow, there exists a laminar sublayer, where heat transfer takes place through laminar convection. The thickness of this laminar sublayer is usually neglected in turbulent heat transfer calculation, which may not be negligible in microscale flow. As a result, although calculations were performed assuming turbulent flow, it is possible that a small fraction of the flow area actually had turbulent convection while the rest had laminar convection only, causing the large deviation from macroscale correlations.

The uncertainties associated with Nusselt number measurements varied from 20% to 67%. As before, the uncertainty was higher for lower flow rates. However, the uncertainties associated with temperature measurements specifically at test-section inlet and outlet were the dominating factors in this case. The order of magnitude of temperature measurement uncertainty was 3-4 times higher compared with the contribution of other parameters involved in the calculation of Nusselt number. Since

Nusselt number calculations involved temperature differences, at lower flow rate uncertainties were higher due to small temperature difference while the opposite was true for high flow rates. This phenomenon can be observed from the error bars associated with Nusselt number measurements.

A comparison has been made of the experimental data with the correlation proposed by Peng *et al.* (1994). Although their experimental data were limited to  $Re \leq 3000$ , those results have been extrapolated to match the Reynolds numbers of the present study. Based on the hydraulic diameters of the microchannels two different coefficients were used to plot the Peng *et al.* (1994) data. The experimental data did not agree quite well with the proposed correlation. It was apparent that two different factors that affect heat transfer were present in the microchannels considered in this study. For the two smaller channels the experimental data agreed reasonably well for Reynolds numbers within the scope of Peng's original research. However, for the two larger channels in this study, heat transfer rate was much higher than the smaller channels. This may be attributed to a much higher surface roughness for the larger channels. However, it is not clear whether this higher rate of heat transfer was achieved due to larger hydraulic diameter or higher surface roughness of the microchannels. Also it could not be ascertained whether the disagreement of the experimental data for the larger channels with Peng *et al.*'s (1994) correlation was due to the extrapolation of the correlation to a much higher Reynolds number or for any other reason.

### **Recommendations for Future Research**

It was mentioned in the beginning that the primary goal of this study is to develop a better understanding of the fluid flow and heat transfer phenomena in microchannels. Although this study may have helped us to gain further insight in this area, much more research needs to be done. As a continuation of the present study one may look into the aspects of turbulence modeling inside microchannels to see whether turbulence mixing is restricted by the physical size of the microchannels and thus suppressing the heat transfer mechanism associated with it. Studies of single- and two-phase flow using localized temperature and pressure measurements will definitely provide further insight into this field. As discussed in the previous chapter temperature measurements are crucial for Nusselt number calculation. The inaccuracies in the thermocouples had a major contribution in Nusselt number uncertainty, which was as high as 67%. It is expected that advanced fabrication techniques will make localized instrumentation possible in the near future. It may be worthwhile to examine the effect of channel geometry on the two parameters studied. Considering the increasing need for heat dissipation from electronic devices and other microfluidic equipment, the need for basic research in the micro thermo-fluid area will continue to have far reaching effect for all areas of micro technologies.

**APPENDIX**  
**EXPERIMENTAL DATA**

**Measured Data for Channel B**

Number of Channels: 3

Channel Dimensions:

Depth: 211.1 E-6 m

Width: 208.9 E-6 m

Length: 0.0635 m

Hydraulic Diameter: 210.6 E-6 m

Data point	Test Fixture Temperature (°C)		Temp. Wall	Test Fixture Pressure (Pa)		Flow Rate (cc/min)
	Inlet	Outlet		Inlet	Outlet	
1	17.91	21.34	23.84	786413.7931	767475.86	14.76
2	17.96	22.65	25.61	851586.2069	768482.76	27.36
3	18.11	23.70	29.15	938965.5172	769310.34	41.25
4	18.20	24.83	31.90	1069172.414	771020.69	57.45
5	18.24	25.67	35.04	1171448.276	773558.62	68.03
6	18.27	26.30	39.34	1258206.897	775034.48	76.00
7	18.36	26.11	41.38	1352896.552	774937.93	83.81
8	18.44	26.01	44.54	1426551.724	773172.41	89.51



**Calculated Data for Channel B**

Number of Channels: 3

Channel Dimensions:

Depth: 211.1 E-6 m

Width: 208.9 E-6 m

Length: 0.0635 m

Hydraulic Diameter: 210.6 E-6 m

Data point	Velocity (m/s)	Re	f	Heat Flux W/m <sup>2</sup>	Heat Trans.	Nu	% Uncertainty	
					coeff. W/m <sup>2</sup> -K		U_f	U_Nu
1	1.87	2119.58	0.02429	12073.00	2866.79	7.15	19.32	53.20
2	3.47	3958.68	0.03237	30565.41	5760.18	14.42	18.47	40.28
3	5.24	6010.25	0.02851	55108.57	6687.93	16.80	9.37	30.54
4	7.31	8428.88	0.02531	90944.84	8752.83	22.06	5.75	25.30
5	8.66	10030.90	0.02382	120758.57	9231.19	23.32	4.71	21.87
6	9.69	11250.18	0.02302	145740.29	8544.02	21.63	4.19	19.46
7	10.68	12393.40	0.02259	154865.11	8088.36	20.47	3.31	19.70
8	11.40	13232.74	0.02235	161723.44	7249.22	18.35	3.08	19.95

**Measured Data for Channel C1**

Number of Channels: 5

Channel Dimensions:

Depth: 134.6 E-6 m

Width: 121.8 E-6 m

Length: 0.0635 m

Hydraulic Diameter: 127.9 E-6 m

Data point	Test Fixture Temperature (°C)		Temp. Wall	Test Fixture Pressure (Pa)		Flow Rate (cc/min)
	Inlet	Outlet		Inlet	Outlet	
1	21.06	23.39	29.07	824896.5517	776965.52	8.89
2	21.22	23.99	30.68	892482.7586	765862.07	18.25
3	21.76	24.90	32.14	974827.5862	770068.97	21.86
4	22.12	25.84	33.89	1041103.448	766344.83	23.94
5	22.11	26.86	34.26	1211103.448	775931.03	31.65
6	21.28	26.29	34.58	1315931.034	772758.62	35.49
7	21.42	26.91	35.38	1399655.172	775544.83	38.82

### Calculated Data for Channel C1

Number of Channels: 5

Channel Dimensions:

Depth: 134.6 E-6 m

Width: 121.8 E-6 m

Length: 0.0635 m

Hydraulic Diameter: 127.9 E-6 m

					Heat Trans.		% Uncertainty	
Data	Velocity	Re	f	Heat Flux	coeff.	Nu	U_f	U_Nu
point	(m/s)			W/m <sup>2</sup>	W/m <sup>2</sup> -K			
1	1.81	1282.62	0.04517	4800.58	700.79	1.08	13.14	65.15
2	3.73	2642.83	0.02719	11666.38	1445.32	2.23	12.86	54.63
3	4.47	3185.95	0.03110	15864.42	1800.15	2.79	8.94	48.67
4	4.90	3516.15	0.03507	20556.92	2073.40	3.23	7.37	41.82
5	6.49	4672.49	0.03149	34760.50	3554.76	5.55	5.14	33.94
6	7.28	5210.67	0.03114	41073.20	3803.90	5.92	4.02	31.63
7	7.96	5722.28	0.02977	49250.37	4393.89	6.85	3.89	29.35

**Measured Data for Channel C2**

Number of Channels: 3

Channel Dimensions:

Depth: 263.7 E-6 m

Width: 170.4 E-6 m

Length: 0.0635 m

Hydraulic Diameter: 207.0 E-6 m

Data point	Test Fixture Temperature (°C)		Temp. Wall	Test Fixture Pressure (Pa)		Flow Rate (cc/min)
	Inlet	Outlet		Inlet	Outlet	
1	17.88	21.97	24.93	787172.4138	770937.93	14.03
2	17.98	23.75	27.24	876206.8966	774386.21	31.75
3	18.10	24.58	28.92	953103.4483	774924.14	43.12
4	17.96	24.83	29.64	1027517.241	771200.00	53.35
5	18.04	24.74	31.41	1094551.724	772717.24	61.84
6	18.11	25.14	33.11	1196275.862	774579.31	71.52
7	17.96	25.54	36.35	1322758.621	774717.24	81.17
8	18.07	25.93	38.14	1413310.345	774979.31	91.28

**Calculated Data for Channel C2**

Number of Channels: 3

Channel Dimensions:

Depth: 263.7 E-6 m

Width: 170.4 E-6 m

Length: 0.0635 m

Hydraulic Diameter: 207.0 E-6 m

					Heat Trans.		% Uncertainty	
Data	Velocity	Re	f	Heat Flux	coeff.	Nu	U_f	U_Nu
point	(m/s)			W/m <sup>2</sup>	W/m <sup>2</sup> -K			
1	1.75	1957.26	0.02346	12382.14	2473.58	6.09	22.34	45.05
2	3.96	4477.76	0.02975	39514.30	6198.73	15.34	14.81	33.16
3	5.38	6112.27	0.02796	60302.23	7953.08	19.74	8.68	28.81
4	6.67	7571.89	0.02594	79101.40	9592.41	23.82	6.17	26.89
5	7.72	8771.78	0.02395	89368.16	8915.57	22.14	5.03	25.50
6	8.93	10166.81	0.02338	108551.48	9450.42	23.50	4.07	23.73
7	10.15	11560.37	0.02359	132704.39	9085.25	22.60	3.67	21.30
8	11.42	13033.98	0.02134	154847.40	9594.06	23.90	2.82	20.16

**Measured Data for Channel D**

Number of Channels: 7

Channel Dimensions:

Depth: 111.3 E-6 m

Width: 112.4 E-6 m

Length: 0.0635 m

Hydraulic Diameter: 111.8 E-6 m

Data point	Test Fixture Temperature (°C)		Temp. Wall	Test Fixture Pressure (Pa)		Flow Rate (cc/min)
	Inlet	Outlet		Inlet	Outlet	
1	17.82	21.49	24.92	852827.5862	773131.03	11.83
2	17.91	21.64	25.68	907724.1379	773324.14	19.25
3	18.08	23.67	29.40	1026206.897	774703.45	24.72
4	18.13	24.29	32.12	1106965.517	775075.86	27.43
5	18.31	25.88	36.29	1303586.207	775806.90	32.13
6	18.50	26.36	38.81	1363034.483	775186.21	33.16
7	18.58	26.63	40.61	1408344.828	775462.07	36.76

**Calculated Data for Channel D**

Number of Channels: 7

Channel Dimensions:

Depth: 111.3 E-6 m

Width: 112.4 E-6 m

Length: 0.0635 m

Hydraulic Diameter: 111.8 E-6 m

					Heat Trans.		% Uncertainty	
Data	Velocity	Re	f	Heat Flux	coeff.	Nu	U_f	U_Nu
point	(m/s)			W/m <sup>2</sup>	W/m <sup>2</sup> -K			
1	2.26	1368.58	0.04203	8360.35	1588.36	2.11	23.37	67.00
2	3.68	2229.62	0.02581	13812.73	2340.35	3.11	15.81	57.02
3	4.74	2898.36	0.02959	26584.43	3116.79	4.17	9.75	38.46
4	5.27	3227.92	0.03189	32559.47	2986.92	4.00	7.92	33.03
5	6.19	3818.82	0.03730	46870.70	3300.50	4.45	6.55	27.97
6	6.39	3956.12	0.03910	50236.77	3065.71	4.14	8.03	31.40
7	7.08	4391.24	0.03396	57081.37	3171.01	4.28	6.73	27.62

## BIBLIOGRAPHY

- Adams, T.M., Abdel-Khalik, S.I., Jeter, S.M. and Qureshi, Z.H., "An Experimental Investigation of Single-Phase Forced Convection in Microchannels" – International Journal of Heat and Mass Transfer, Vol. 41, Nos 6-7, 1998, pp. 851-857.
- Arkilic, E.B., Breur, K.S. and Schmidt, M.A., "Gaseous Flow in Microchannels" - ASME, FED-Vol. 197, Application of Microfabrication to Fluid Mechanics, 1994, pp. 57-66.
- Babin, B.R., Peterson, G.P. and Wu, D., "Steady-state Modeling and Testing of a Micro Heat Pipe" - Journal of Heat Transfer, Vol. 112, August 1990, pp. 595-601.
- Bailey, Darin K., "An Apparatus for the Study of Friction and Heat Transfer in Microchannels" - MS thesis, Louisiana Tech University, 1996.
- Baker, Ovid, "Simultaneous Flow of Oil and Gas" – The Oil and Gas Journal, July 1954, pp. 185-195.
- Barron, R.F., "Cryogenic Systems" - 2<sup>nd</sup> edition, Oxford University Press, 1985.
- Bhatti, M.S. and Shah, R.K., "Handbook of Single-Phase Convective Heat Transfer", Chapter 4, edited by S. Kakac, R.K. Shah, and W. Aung, John Wiley and Sons, 1987.
- Bowers, M.B. and Mudawar, I., "Two-Phase Electronic Cooling Using Minichannel and Microchannel Heat Sinks: Part 1- Design Criteria and Heat Diffusion Constraints" - ASME Transactions, Journal of Electronic Packaging, Vol. 116, December 1994a, pp. 290-297.
- Bowers, M.B. and Mudawar, I., "Two-Phase Electronic Cooling Using Minichannel and Microchannel Heat Sinks: Part 2- Flow Rate and Pressure Drop Constraints" - ASME Transactions, Journal of Electronic Packaging, Vol. 116, December 1994b, pp. 298-305.
- Choi, S.B., Barron, R.F. and Warrington, R.O., "Fluid Flow and Heat Transfer in Microtubes" - ASME, DSC - Vol. 32, Micromechanical Sensors, Actuators and Systems, 1991, pp. 123-134.



- Chyu, M-C. and Zaidi, S.H.R., "Characteristics of Boiling Heat Transfer in a Narrow Gap" - ASME, HTD - Vol. 145, Single and Multiphase Convective Heat Transfer, 1990, pp. 47-53.
- Flockhart, S.M. and Dhariwal, R.S., "Experimental and Numerical Investigation into the Flow Characteristics of Channels Etched in <100> Silicon" - Journal of Fluids Engineering, Vol. 120, June 1998, pp. 291-295.
- Harley, J.C., Huang, Y., Bau, H.H. and Zemel, J.N., "Gas Flow in Microchannels" - Journal of Fluid Mechanics, Vol. 284, 1995, pp. 257-274.
- Incropera, F.P. and DeWitt, D.P., "Fundamentals of Heat and Mass Transfer" - 4<sup>th</sup> edition, John Wiley and Sons, 1996.
- Kays, W.M., "Loss Coefficients for Abrupt Changes in Flow Cross Section with Low Reynolds Number Flow in Single and Multiple-Tube Systems" - ASME Transactions, 1950, pp. 1067-1074.
- Kays, W.M. and Crawford, M.E., "Convective Heat and Mass Transfer" - 3<sup>rd</sup> edition, McGraw-Hill, Inc., 1993.
- Kishimoto, T. and Ohsaki, T., "VLSI Packaging Technique Using Liquid Cooled Channels" - Proceedings of IEEE, 1986, pp. 595-601.
- Knudsen, M., "Die Gesetze Der Molecular Stromung Und Die Inneren Reibungstromung Der Gase Durch Rohren", Annalen der Physik, Vol. 28, 1909, pp. 75-130.
- Kreith, F., "Principles of Heat Transfer" - 3<sup>rd</sup> edition, 1970.
- Lin, L., Udell, K.S. and Pisano, A.P., "Vapor Bubble Formation on a Micro-Heater in Confined and Unconfined Microchannels" - ASME, HTD - Vol.253, Heat Transfer on the Microscale 1993, pp. 85-93.
- Ma, S.W. and Gerner, F.M., "Forced Convection Heat Transfer from Microstructures" - Transactions of the ASME, Vol. 115, Nov. 1993, pp. 872-880.
- Mallik, A.K., Peterson, G.P. and Weichold, M.H., "On the Use of Micro Heat Pipes as an Integral Part of Semiconductor Devices" - ASME Transactions, Journal of Electronic Packaging, Vol. 114, Dec. 1992, pp. 436-442.
- Orozco, J. and Hanson, C., "A Study of Mixed Convection Boiling Heat Transfer in Narrow Gaps" - ASME, HTD - Vol. 206-2, Topics in Heat Transfer, 1992, pp. 81-85.

- Papautsky, I., Gale, B.K., Mohanty, S., Ameer, T.A. and Frazier, A.B., "Effects of Rectangular Microchannel Aspect Ratio on Laminar Friction Constant" - SPIE Vol. 3877, September 1999, pp. 147-158.
- Peng, X.F., personal communication, 1995.
- Peng, X.P., Hu, H.Y. and Wang, B.X., "Boiling Nucleation During Liquid Flow in Microchannels" - International Journal of Heat and Mass Transfer, Vol. 41, No. 1, 1998a, pp. 101-106.
- Peng, X.P., Hu, H.Y. and Wang, B.X., "Flow Boiling Through V-Shape Microchannels" - Experimental Heat Transfer, Vol. 11, 1998b, pp. 87-100.
- Peng, X.F. and Peterson, G.P., "Convective Heat Transfer and Flow Friction for Water Flow in Microchannel Structures" - International Journal of Heat and Mass Transfer, Vol. 39, No. 12, 1996, pp. 2599-2608.
- Peng, X.F., Peterson, G.P. and Wang, B.X., "Frictional Flow Characteristics of Water Flowing Through Rectangular Microchannels" - Experimental Heat Transfer, Vol. 7, 1994a, pp. 249-264.
- Peng, X.F., Peterson, G.P. and Wang, B.X., "Heat Transfer Characteristics of Water Flowing Through Rectangular Microchannels" - Experimental Heat Transfer, Vol. 7, 1994b, pp. 265-283.
- Peng, X.F. and Wang, B.X., "Liquid Flow and Heat Transfer in Microchannels with/without Phase Change" - Invited paper, 10th International Heat Transfer Conference, Aug. 14-18, 1994, Brighton, UK, pp. 159-177.
- Peng, X.F., Wang, B.X., Peterson, G.P. and Ma, H.B., "Experimental Investigation of Heat Transfer in Flat Plates with Rectangular Microchannels" - International Journal of Heat and Mass Transfer, Vol. 38, No. 1, 1995, pp. 127-137.
- Peterson, G.P., Duncan, A.B., Ahmed, A.S., Mallik, A.K. and Weichold, M.H., "Experimental Investigation of Micro Heat Pipes in Silicon Wafers" - ASME, DSC - Vol. 32, Micromechanical Sensors, Actuators and Systems, 1991, pp.341-348.
- Peterson, G.P., Duncan, A.B. and Weichold, M.H., "Experimental Investigation of Micro Heat Pipes Fabricated in Silicon Wafers" - Journal of Heat Transfer, Vol. 115, August 1993, pp. 751-756.
- Pfahler, J., Harley, J., Bau, H.H. and Zemel, J., "Liquid and Gas Transport in Small Channels" - ASME, DSC - Vol. 119, 1990, pp. 149-157.

- Pfahler, J., Harley, J., Bau, H. and Zemel, J.N., "Gas and Liquid Flow in Small Channels" - ASME, DSC - Vol. 32, Micromechanical Sensors, Actuators and Systems, 1991, pp. 49-60.
- Pong, K-C., Ho, C-M., Liu, J. and Tai, Y-C., "Non-Linear Pressure Distribution in Uniform Microchannels" - ASME, FED - Vol. 197., Application of Microfabrication to Fluid Mechanics, 1994, pp. 51-56.
- Ravigururajan, T.S., "Impact of Channel Geometry on Two-Phase Flow Heat Transfer Characteristics of Refrigerants in Microchannel Heat Exchangers" - Journal of Heat Transfer, Vol. 120, May 1998, pp. 485-491.
- Schonberg, J.A., Dasgupta, S. and Wayner, P.C., Jr., "An Augmented Young-Laplace Model of an Evaporating Meniscus in a Microchannel with High Heat Flux" - Experimental Thermal and Fluid Science, 1995, Vol. 10, pp. 163-170.
- Shah, R.K. and Bhatti, M.S., "Handbook of Single-Phase Convective Heat Transfer", Chapter 3, edited by S. Kakac, R.K. Shah, and W. Aung, John Wiley and Sons, 1987.
- Shah, R.K. and London, A.L., "Laminar Flow Forced Convection in Ducts" - Supplement 1, Advances to Heat Transfer, Academic Press, New York, 1978.
- Stanley, Roger S., "Two Phase Flow in Microchannels" - Doctor of Engineering dissertation, Louisiana Tech University, 1997.
- Tong, L.S. and Tang, Y.S., "Boiling Heat Transfer and Two-Phase Flow" - 2<sup>nd</sup> edition, Taylor and Francis, 1997.
- Tuckerman, D.B. and Pease, R.F.W., "High Performance Heat Sinking for VLSI" - IEEE Electronic Device Letters, Vol. EDL-2, No. 5, May 1981, pp. 126-129.
- Wang, C. and Beckerman, C., "A Two-Phase Mixture Model of Liquid-Gas Flow and Heat Transfer in Capillary Porous Media - I. Formulation" - International Journal of Heat and Mass Transfer, Vol. 36, No. 11, 1993, pp. 2747-2758.
- Wang, C. and Beckerman, C., "A Two-Phase Mixture Model of Liquid-Gas Flow and Heat Transfer in Capillary Porous Media - II. Application to Pressure Driven Boiling Flow Adjacent to a Vertical Heated Plate" - International Journal of Heat and Mass Transfer, Vol. 36, No. 11, 1993, pp. 2759-2768.
- Webb, R.L. and Zhang, M., "Heat Transfer and Friction in Small Diameter Channels" - Microscale Thermophysical Engineering, Vol. 2, 1998, pp. 189-202.

Wheeler A.J. and Ganji, A.R., "Introduction to Engineering Experimentation" – Prentice Hall, 1996.

White, F.M., "Viscous Fluid Flow" – 2<sup>nd</sup> edition, McGraw-Hill, Inc., 1991.

Xia, C., Guo, Z. and Hu, W., "Mechanism of Boiling Heat Transfer in Narrow Channels" - ASME, HTD - Vol. 197, Two Phase Flow and Heat Transfer, 1992, pp. 111-119.

Yu, D., Warrington, R.O., Barron, R.F. and Ameel, T.A., "An Experimental and Theoretical Investigation of Fluid Flow and Heat Transfer in Microtubes" - Invited Paper, ASME/JSME International Thermal Engineering Conference, 1994, Maui, Hawaii, USA.

Zhao, Y., Molki, M., Ohadi, M.M. and Dessiatoun, S.V., "Flow Boiling of CO<sub>2</sub> in Microchannels" - ASHRAE Transactions, Vol. 106, Pt. 1, 2000, pp. 1-9.

## **VITA**

Mr. Abdullahel Bari was born in Dhaka, Bangladesh, and grew up in the same city. He received his BSME from Bangladesh University of Engineering and Technology in 1988 and MSME from Oklahoma State University in 1992. In Fall 1995 he came to Louisiana Tech University as a doctoral student in the Department of Mechanical Engineering. Mr. Bari conducted his dissertation research in the area of microfluidics at the Institute for Micromanufacturing. As a graduate student, he was a research assistant and an instructor for the Department of Mechanical Engineering.